Interannual variability of summertime formaldehyde (HCHO) vertical column density and its main drivers in northern high latitudes

Style Definition: Comment Text

Tianlang Zhao[1], Jingqiu Mao[1], Zolal Ayazpour[2,3], Gonzalo González Abad[3], Caroline R Nowlan[3], Yiqi Zheng[1]

[1] University of Alaska Fairbanks, Department of Chemistry and Biochemistry & Geophysical Institute, Fairbanks, AK, United States

[2] University at Buffalo, Department of Civil, Structural and Environmental Engineering, Buffalo, NY, United States

[3] Center for Astrophysics, Harvard & Smithsonian, Cambridge, MA, United States

Correspondence to: Tianlang Zhao (tzhao@alaska.edu) and Jingqiu Mao (jmao2@alaska.edu)

Deleted: ¶

Abstract:

The northern high latitudes (50-90°N, mostly including boreal forest and tundra ecosystem) has been undergoing rapid climate and ecological changes over recent decades, leading to significant variations in Volatile Organic Compounds (VOCs) emissions from biogenic and biomass burning sources. Formaldehyde (HCHO) is an indicator of VOC emissions, but the interannual variability of HCHO and its main drivers over the region remain unclear. In this study, we use the GEOS-Chem chemical transport model and satellite retrievals from Ozone Monitoring Instrument (OMI) and Ozone Mapping and Profiler Suite (OMPS), to examine the interannual variability of HCHO vertical column density (VCD) during the summer seasons spanning from 2005 to 2019. Our

Deleted: volatile organic compounds

Deleted: , a widely used

Deleted: emission, exhibits high climate sensitivity. However,…

Deleted:)

Deleted: interannual variations in summertime of

Deleted: -

results show that in 2005-2019 summers, wildfires contribute 75-90% of the interannual variability of HCHO VCD over Siberia, Alaska, and Northern Canada, while biogenic emissions and background methane oxidation accounts for ~90% of HCHO interannual variability over Eastern Europe. We find that monthly Solar-induced chlorophyll fluorescence (SIF) from Orbiting Carbon Observatory-2 (OCO-2), an efficient proxy for plant photosynthesis, shows a good linear relationship (R=0.6-0.7) with modelled biogenic HCHO column ($dVCD_{Bio,GC}$) in Eastern Europe, Siberia, Alaska and Northern Canada, indicating the coupling between SIF and biogenic VOC emissions over the four domains on a monthly scale. In Alaska, Siberia and Northern Canada, SIF and $dVCD_{Bio,GC}$ both show a relatively lower interannual variabilities (SIF: CV=1-9%, $dVCD_{Bio,GC}$: CV=1-2%. CV: Coefficient of Variation) comparing to wildfire-induced HCHO (CV=8-13%), suggesting that the high interannual variabilities of OMI HCHO VCD (CV=10-16%) in these domains are likely driven by wildfires instead of biogenic emissions.

Deleted: heavily influence

Deleted: North

Deleted: are the predominant drivers

Deleted: East

Deleted:) provides additional evaluation for HCHO interannual variability from

Deleted: emission, showing potential of constraining

Deleted: emission in northern

Formatted: English (UK)

Deleted: latitudes

Formatted: Font: Not Bold

1. Introduction

VOCs are main precursors of tropospheric ozone and secondary organic aerosols, strongly impacting air quality and climate (Atkinson, 2000; Kroll and Seinfeld, 2008; Mao et al., 2018; Zheng et al., 2020). HCHO is mainly produced from atmospheric VOC oxidation with a short photochemical lifetime on the order of hours, serving as an indicator of non-methane VOC (NMVOC) emissions and photochemical processes (Fu et al., 2007; Millet et al., 2008). Understanding the interannual variability of HCHO is important for quantifying long-term trend of VOC emissions in response to climate changes and air quality control implementation.

Deleted: (Jin et al., 2017; Mao et al., 2018; Jin et al., 2020; Zheng et al., 2020)

Several studies suggest that biogenic VOC emissions are largely responsible for interannual variabilities of HCHO on a global scale (Palmer et al., 2001; De Smedt et al., 2008; González Abad et al., 2015; De Smedt et al., 2018). Stavrakou et al. (2009) attributes Biogenic VOCs (BVOCs) emissions as the predominant source of global HCHO columns, in which isoprene alone contributes to 30% of global HCHO. Isoprene emissions were also found to be the major driver of HCHO interannual variability (Bauwens et al., 2016; Stavrakou et al., 2018; Morfopoulos et al., 2022). During wildfire seasons, pyrogenic emission is the secondary important controlling factor of HCHO over the whole Amazon (Zhang et al., 2019) and contributes to 50-72% of HCHO total column in Alaskan summer fire seasons (Zhao et al., 2022). Over Antarctic region, HCHO is produced mainly from methane oxidation with hydroxyl radicals (OH), with possible unknown HCHO sources and long-range transport (Riedel et al., 1999). The interannual variability of HCHO over this region is still unclear.

Deleted: , according to model estimation

Deleted: Pyrogenic and anthropogenic sources can also contribute to a large part of HCHO in regional scales, such as in the

Deleted: Alaska (Zhao et al., 2022).

Formatted: English (US)

Formatted: English (US)

Northern high latitudes are experiencing rapid Arctic warming in recent decades, resulting in strong increases in BVOC emissions (Lappalainen et al., 2009; Vedel-Petersen et al., 2015; Kramshøj et al., 2016; Seco et al., 2022). Several studies suggest monoterpenes to be the most abundant BVOC species in boreal forests over middle and north Europe, and southeastern Siberia (Spirig et al., 2004; Timkovsky et al., 2010; Bäck et al., 2012; Rantala et al., 2015; Juráň et al., 2017; Zhou et al., 2017). This BVOC speciation appears to be different in the boreal forests in Alaska, Northern Canada and Eastern Siberia, where isoprene appears to be the most abundant BVOC species (Blake et al., 1992; Timkovsky et al., 2010; Zhao et al., 2022). BVOC measurements in tundra systems show a very strong positive temperature dependence for isoprene fluxes, over Greenland (Vedel-Petersen et al., 2015; Kramshøj et al., 2016; Lindwall et al., 2016a),

Deleted: predominant

Formatted: Font: Times New Roman

Deleted: (Rinne et al., 2000; Spirig et al., 2004; Timkovsky et al., 2010; Bäck et al., 2012; Rantala et al., 2015; Juráň et al., 2017; Zhou et al., 2017).

Deleted: North

Deleted: East

Deleted: predominant

Formatted: Spanish (Traditional Sort)

Deleted:

Deleted: system

Deleted:

northern Sweden (Faubert et al., 2010; Tang et al., 2016) and the Alaskan North Slope (Potosnak et al., 2013; Angot et al., 2020; Selimovic et al., 2022).

Deleted: Whether or not these changes can be seen from satellite HCHO observations remains unclear.

Formatted: English (US)

Wildfire is another important source of HCHO (Permar et al., 2021). A number of studies have shown positive trend and strong interannual variability of wildfires over Arctic regions in the past few decades (Kelly et al., 2013; Giglio et al., 2013; Descals et al., 2022). Several modelling studies suggest that wildfires can become the main source of HCHO over Alaska (Zhao et al., 2022), Siberia and Canada (Stavrakou et al., 2018). In fact, the contribution from wildfires could be even larger as models tend to underestimate the secondary production of HCHO from other VOC precursors (Alvarado et al., 2020; Zhao et al., 2022; Jin et al., 2023). To what extent wildfires contribute to HCHO interannual variability remains unclear.

Deleted: major

Deleted: of VOCs with large direct emissions

Deleted: , suggesting an increasingly important role of wildfires on HCHO sources.

Solar Induced Fluorescence (SIF) could potentially provide additional constraints on biogenic-related HCHO column over northern high latitudes, due to their similar dependence on temperature and light availability (Foster et al., 2014; Zheng et al., 2015). SIF is the re-emission of light by plants as a result of absorbing solar radiation during photosynthesis and is widely used to estimate vegetation productivity and health (Porcar-Castell et al., 2014; Magney et al., 2019). Isotopic labeling studies show that 70-90% of isoprene production is from chloroplasts, directly linked to photosynthesis (Delwiche and Sharkey, 1993; Karl et al., 2002; Affek and Yakir, 2003). As SIF is directly linked to flux-derived Gross Primary Productivity (GPP) and HCHO can be largely explained by isoprene emissions (Zheng et al., 2017), we expect to use SIF as a valuable tool to constrain biogenic emissions from boreal forest at northern high latitudes.

Deleted: Satellite

Formatted

Formatted: Font color: Accent 1

Deleted: some correlation between satellite observations of HCHO and SIF under certain conditions.

The new retrievals of HCHO from OMI and OMPS provide a continuous long-term record on a global scale, with improved calibration, updates in spectral fitting and air mass factor calculations (González Abad et al., 2022; Nowlan et al., 2023). Here we use the newly retrieved HCHO vertical column density (VCD) products from OMI and OMPS, combined with GEOS-Chem chemical transport model, to examine summertime HCHO spatiotemporal variability over northern high latitudes from 2005 to 2019. The satellites and the model are introduced in Sect. 2. In Sect. 3, we evaluate the spatial variability of HCHO VCD using satellite retrievals and evaluate BVOC emissions with previous in-situ measurements. In Sect. 4, we evaluate the interannual variability of HCHO VCD using satellite retrievals, and present model sensitivity tests to demonstrate how background HCHO, wildfire and biogenic VOC emissions influence HCHO interannual variability across Alaska, Siberia, Northern Canada and Eastern Europe. In Sect. 5, we evaluate biogenic HCHO interannual variability using satellite SIF data. Summary and discussion are in Sect. 6.

Deleted: Here we use newly retrieved HCHO vertical column density (VCD) products from OMI and OMPS, combined with GEOS-Chem chemical transport model, to examine summertime HCHO spatiotemporal variability over northern high latitudes from 2005 to 2019. The satellites and the model are introduced in section 2. In section 3, we evaluate spatial and interannual variability of modelled HCHO VCD using OMI and OMPS retrievals. Section 4 presents model sensitivity tests, demonstrating how background HCHO, wildfire and biogenic VOC emissions influence HCHO interannual variability across Alaska, Siberia, North Canada and East Europe in northern high latitudes. In section 5, we evaluate biogenic HCHO interannual variability using satellite SIF data. Summary and discussion are in section 6.¶

2. Observations and Model

2.1. Observational data sets

We use satellite observations of tropospheric HCHO columns from OMI and OMPS to evaluate summertime HCHO variability at northern high latitudes. OMI is a UV/Visible backscatter spectrometer on-board the Aura satellite launched in July 2004, with global daily coverage at an overpass time of 13:30 LT. OMI provides a long-term record of HCHO VCD but is discontinued in 2023. OMPS is the continuation of OMI HCHO measurement over polar region. OMPS is a spectrometer on-board two satellites: NASA/NOAA SUOMI NPP (hereafter SNPP) and NOAA-20, which were launched in October 2011 and November 2017, respectively. Compared to OMI,

Deleted: in

Deleted: The

OMPS-SNPP is in a relatively lower nadir spatial resolution (OMI: 13×24 km^2, OMPS-SNPP: 50×50 km^2) (de Graaf et al., 2016; Levelt et al., 2006) but has an improved signal-to-noise ratio (González Abad et al., 2016). OMI and OMPS HCHO products share a similar concept and retrieval approach, so the joint evaluation by the two satellites can examine the consistency between OMI and OMPS and, more importantly, provide capability to study HCHO interannual variability on a decadal timescale. Here we use monthly mean HCHO VCD from OMI HCHO VCD retrieval (OMHCHO Version-4) product (González Abad et al., 2022) during 2005-2019 summertime, and OMPS-SNPP Level 2 HCHO total column V1 product (Nowlan et al., 2023) during 2012-2019 summertime, provided by the Smithsonian Astrophysical Observatory.

The OMI and OMPS HCHO retrievals use a three-step procedure to calculate the HCHO VCD (Nowlan et al., 2023). First, the slant column density (SCD) is determined through spectral fitting of a backscattered radiance spectrum collected in the wavelength region of 328.5 to 356.5 nm. This fit uses a daily reference spectrum (one for each cross-track position) determined from radiances collected over a relatively clean area of the Pacific between latitudes 30°S and 30°N. The area used for this reference calculation is referred to as the reference sector. Second, scene-by-scene radiative transfer calculations are performed to determine vertically-resolved scattering weights, which can be used to determine the air mass factor (AMF) in combination with the trace gas profile (Palmer et al., 2001). This AMF describes the path of light and is used for converting the SCD to a VCD (VCD=SCD/AMF). Third, the background reference slant column (SCD_R) in the radiance sector region is determined using a model, to correct the retrieved SCD which is in fact the differential SCD determined from the ratio of the observed radiance and the reference

Deleted: of

Deleted: and OMPS-SNPP are

Deleted: and

Deleted: respectively

Formatted: English (UK)

Deleted: . Here we use OMI data from 2005 to 2019 and OMPS-SNPP data from 2012 to 2019. We calculate

Formatted: English (UK)

Formatted: English (UK)

Formatted: English (UK)

radiance. A further bias correction (SCD_B) is applied to reduce high-latitude biases, which mostly affect OMPS-SNPP (Nowlan et al., 2023).

To compare with modelled results, OMI and OMPS-SNPP HCHO retrievals are reprocessed following a three-step procedure. This is primarily done to replace the climatology used in the OMI and OMPS-SNPP products with our own GEOS-Chem simulations. First, we remove the data points falling in the following criteria: (1) main quality flag > 0, (2) cloud cover fraction ≥ 40%, (3) solar zenith angle (SZA) ≥ 70°, and (4) Ice/snow flag = 1. After filtering, we regrid the level 2 swath data in the local time window 12:00–15:00 LT to 0.5°×0.625° horizontal resolution. Second, we calculate the air mass factor (AMF_{GC}) based on local GEOS-Chem HCHO vertical profile and satellite scattering weight (Palmer et al., 2001). Third, we calculate the slant column density of HCHO in the reference sector ($SCD_{R,SAT}$), using modelled HCHO reference sector column and satellite air mass factor over the same location ($VCD_{R,GC}$ and $AMF_{R,SAT}$) (De Smedt et al., 2018; Zhu et al., 2016):

Deleted: climatologies

$$SCD_{R,SAT} = VCD_{R,GC} \times AMF_{R,SAT} \qquad (1)$$

$VCD_{R,GC}$ is calculated by global monthly climatology of hourly HCHO profiles at the time of overpass, from a 2018 GEOS-Chem high-performance (GCHP) run at 0.5°×0.5° resolution (Bindle et al., 2021; Eastham et al., 2018). $AMF_{R,SAT}$ is the AMF from the satellite product, which is calculated using the VLIDORT radiative transfer model as described in Nowlan et al. (2023). We rearrange the satellite vertical column as following:

$$VCD_{SAT,reprocessed} = (\Delta SCD_{SAT} + SCD_{B,SAT} + SCD_{R,SAT}) \,/\, AMF_{GC} \qquad (2)$$

Here ΔSCD_{SAT} is the fitted HCHO slant column, $SCD_{B,SAT}$ is the bias correction term for unexplained background patterns in the HCHO retrievals which may be due to instrument or retrieval issues (Nowlan et al., 2023). The single-scene precision of the retrieval is 1×10^{16} molecules cm^{-2} (absolute) for OMI and 3.5×10^{15} molecules cm^{-2} for OMPS-SNPP from spectral fitting and 45–105% (relative) from the AMF (González Abad et al., 2015; Nowlan et al., 2023). The spectral fitting error is primarily random in individual measurements, while the AMF error has both random and systematic components. The precision can be improved by spatial and temporal averaging (De Smedt et al., 2008; Zhu et al., 2016; Boeke et al., 2011). Our analyses in this work are based on monthly data, so the absolute uncertainty in HCHO column is reduced to $<1\times10^{15}$ molecules cm^{-2} (De Smedt et al., 2018).

We utilize high-resolution SIF estimates derived from OCO-2 and MODIS (doi: https://doi.org/10.3334/ORNLDAAC/1863, last accessed: August 10, 2022). These datasets provided globally contiguous daily SIF estimates at a spatial resolution of approximately 0.05° × 0.05° (around 5 km at the equator) and a temporal resolution of 16 days, from September 2014 to July 2020. The dataset was estimated by using an Artificial Neural Network (ANN) trained on the native OCO-2 SIF observations and MODIS BRDF-corrected seven-band surface reflectance along orbits of OCO-2. The ANN model was subsequently used to predict daily mean SIF (mW $m^{-2}nm^{-1}sr^{-1}$) in the gap regions based on MODIS reflectance and land cover. In our study, the OCO-2 SIF estimates are monthly averaged and regridded to 0.1° × 0.1° spatial resolution for the comparison with OMI HCHO VCD, and regridded to 2° × 2.5° spatial resolution when comparing with GEOS-Chem results.

2.2. Global GEOS-Chem simulations

GEOS-Chem, a 3-D global chemical transport model, is used in this study to examine the spatiotemporal variability of HCHO and VOCs across northern high latitudes. The model is driven by the Modern-Era Retrospective analysis for Research and Applications, Version 2 (MERRA-2), provided by the Global Modeling and Assimilation Office (GMAO) at NASA's Goddard Space Flight Center (Rienecker et al., 2011). GEOS-Chem version 12.7.2 is deployed (doi: 10.5281/zenodo.3701669, last access: August 10, 2022) with an update on cloud chemistry (https://github.com/geoschem/geos-chem/issues/906, last access: August 10, 2022). The simulations encompass 15 summers (1 May to 31 August) from 2005 to 2019, at a horizontal resolution of 2°×2.5° and 72 vertical layers from the surface to 0.01 hPa. For all model runs, we use a standard restart file from the GEOS-Chem 1-year benchmark simulation, followed by an additional spinup period of several days to allow adequate representation of HCHO production and loss in the model.

Deleted: (50-90°N).

Deleted: employed

Deleted: http://wiki.seas.harvard.edu/geos-chem/index.php/GEOS-Chem_12#12.7.2

Biomass burning emissions in our simulation are derived from the Global Fire Emission Database (GFED4.1s) inventory (van der Werf et al., 2017; Randerson et al., 2017). Year-specific GFED4.1s inventory is used in each year of the simulation to make sure the representation of the interannual variability in wildfire emissions. Emissions on a 3-hour basis are obtained from MODIS satellite observations, which provide information on fire detection and burning area (Mu et al., 2011; van

Deleted: Biomass burning emissions in our simulation are derived from the Global Fire Emission Database (GFED4.1s) inventory (Giglio et al., 2013). Year-specific GFED4.1s inventory is used in each year of the simulation to make sure the representation of the interannual variability in wildfire emissions. Emissions on a 3-hour basis are obtained from MODIS satellite observations, which provide information on fire detection and burning area (van der Werf et al., 2017). The GFED4.1s inventory reports the HCHO emission factor of 1.86 g/kg dry matter for boreal forest fires and 2.09 g/kg dry matter for temperate forest fires, aligning with recent field measurements (Liu et al., 2017; Permar et al., 2021).¶

der Werf et al., 2017). The GFED4.1s inventory reports the HCHO emission factor of 1.86 g/kg and 2.09 g/kg dry matter for boreal forest and temperate forest fires (Akagi et al., 2011).

BVOC emissions in the study are calculated online (Emission factor maps computed online) using the Model of Emissions of Gases and Aerosols from Nature (MEGAN, v2.1) (Guenther et al., 2006, 2012), as implemented by Hu et al (2015). Terrestrial vegetation for BVOC emissions is based on the plant functional type (PFT) distribution derived from Community Land Model (CLM4) (Lawrence et al., 2011; Oleson et al., 2013). Utilizing online MEGAN simplifies the investigation of the relationship between BVOC emission patterns and PFTs. CLM4 output (Figure S1) suggests two major PFTs over northern high latitudes: broadleaf deciduous boreal shrubs (mainly over the northern and south Alaska, northern Canada and northern Siberia) and needle leaf evergreen boreal trees (mainly over interior Alaska, northern Canada, south Siberia and the northern part of eastern Europe), both with high emission factors in isoprene and low emission factors in monoterpenes. The southern part of Eastern Europe is dominated by croplands and broadleaf deciduous temperate trees. In this work, 'monoterpenes' from model calculation are lumped monoterpenes, including α-pinene, β-pinene, sabinene and carene.

We conducted a model sensitivity test to assess the difference in BVOC emissions and HCHO $dVCD_{Bio,GC}$ due to online versus offline MEGAN applications. The results of the tests show that the use of online MEGAN has a modest impact on monthly ISOPe and MONOe (25-53% for ISOPe in Alaska, Northern Canada and Eastern Europe, 53% for ISOPe in Siberia; 17-24% for MONOe across the four domains), and provide a similar, isoprene-dominated BVOC emission regime over Alaska, Central Siberia, Northern Canada and Eastern Europe, comparing to results

Deleted: .

Formatted: English (US)

Formatted: English (US)

Deleted: north

Deleted: North

Deleted: North

Deleted: North

Deleted: East

Deleted: East

Deleted: include

from using offline MEGAN. The difference in $dVCD_{Bio,GC}$ between using online and offline MEGAN is approximately 13-26%, suggesting a minor impact on $dVCD_{Bio,GC}$ and VCD_{GC} variability over northern high latitudes when using online or offline MEGAN.

In this study, we use the detailed O_3-NO_x-HO_x-VOC chemistry ("tropchem" mechanism) (Park et al., 2004; Mao et al., 2010, 2013), incorporating updates on isoprene chemistry (Fisher et al., 2016). The performance of this version of isoprene chemistry in GEOS-Chem has been extensively evaluated using recent field campaigns and satellite observations over the southeast US (Fisher et al., 2016; Travis et al., 2016), including HCHO production from isoprene oxidation (Zhu et al., 2016, 2020; Kaiser et al., 2018). The ability of GEOS-Chem with this chemistry to reproduce the vertical profiles of HCHO observed during the Alaska summer, as shown in the ATom-1 in-situ campaign, has been demonstrated (Zhao et al., 2022). Under high-NO_x conditions (1 ppbv), HCHO production is rapid, reaching 70-80% of its maximum yield within a few hours, whereas under low-NO_x conditions (0.1 ppbv or lower), it takes several days to reach the maximum yield, and the cumulative yield is approximately 2-3 times lower than that under high-NO_x conditions (Marais et al., 2012).

Deleted: (Fisher et al., 2016)

Deleted: (Fisher et al., 2016; Travis et al., 2016)

To examine the influence of different sources on HCHO columns in northern high latitudes, we conducted four GEOS-Chem simulations, as described in Table 1, to separate modelled HCHO total column (VCD_{GC}) into three parts, including the background column ($VCD_{0,GC}$), biogenic emission induced column ($dVCD_{Bio,GC}$) as well as wildfire emission induced column ($dVCD_{Fire,GC}$):

Deleted: a series of

Deleted: is

Deleted: :

Deleted:), assuming they are independent:

$$VCD_{GC} = VCD_{0,GC} + dVCD_{Bio,GC} + dVCD_{Fire,GC} \quad (3)$$

$VCD_{0,GC}$ is the VCD_{GC} from the GEOS-Chem simulation in which both biogenic and wildfire emissions are turned off. $VCD_{0,GC}$, $dVCD_{Fire,GC}$ and $dVCD_{Bio,GC}$ are derived by Eq. (4a) to (4c):

Deleted: :

$$VCD_{0,GC} = VCD_{GC}(BG) \quad (4a)$$

$$dVCD_{Fire,GC} = VCD_{GC}(All) – VCD_{GC}(NF) \quad (4b)$$

$$dVCD_{Bio,GC} = VCD_{GC}(NF) – VCD_{0,GC} \quad (4c)$$

$$dVCD_{Fire,GC}* = VCD_{GC}(NB) – VCD_{GC}(BG) \quad (4d)$$

$$dVCD_{Bio,GC}* = VCD_{GC}(All) – VCD_{0,GC}(NB) \quad (4e)$$

Deleted: ¶
In Figure 1(a) we display the extent of four domains focused on in this work.

To assess the linearity assumption in Eq. (3), we conducted model sensitivity tests over a one-month period to evaluate the disparity between VCD_{GC} and $VCD_{0,GC}$ + $dVCD_{Fire,GC}$*+ $dVCD_{Bio,GC}$* (derived from Eq.(4a), (4d) and (4e)). The difference between these two terms is less than 14% in northern high latitudes, suggesting a minor importance of the non-linear effect in this area.

Figure 1a defines the four domains focused on in this work. The selection of Alaska domain follows Zhao et al (2022); Eastern Europe and Siberia domains follow Bauwens et al (2016); northern Canada domain follows the North America domain in Bauwens et al (2016) but excluded Alaska.

Deleted: East

To emphasize the key drivers of HCHO interannual variability, we categorize the years spanning from 2005 to 2019 into two distinct groups: “high HCHO years” and “low HCHO years” within each of the four specified domains. For each domain, the years that have above-average May-August sum of regional-averaged monthly OMI $VCD_{SAT,reprocessed}$ is categorized as “high HCHO year”; those years have the value below average is categorized as “low HCHO years”(shown in Table S1).

Deleted: classify

Formatted: English (US)

Deleted: -

Formatted: English (US)

Deleted: for

Deleted: VCD_{GC} will be classified

Deleted: will be classified

Deleted: ”. The classification is

Formatted: English (US)

Deleted: .

Table 1. Configuration of GEOS-Chem global simulations in this study

Simulations	Biogenic emission	Wildfire
Biogenic + wildfire + Background (All)	On	On
Background (BG)	Off	Off
Biogenic + Background (NF)	On	Off
Wildfire + Background (NB)	Off	On

Formatted: English (US)

We use the coefficient of variation (CV) to quantify the interannual variability of summertime HCHO VCD. CV is defined as the ratio of the standard deviation to the mean ($CV = \frac{\sigma}{\mu}$), which is a measure of interannual variability (Giglio et al., 2013). Assuming $VCD_{0,GC}$, $dVCD_{Bio,GC}$, $dVCD_{Fire,GC}$ are three independent components of VCD_{GC}, we have $\sigma^2_{VCD_{GC}} = \sigma^2_{VCD_{0,GC}} + \sigma^2_{dVCD_{Bio,GC}} + \sigma^2_{dVCD_{Fire,GC}}$, so the contribution of each component to the CV of VCD_{GC} can be calculated by:

$$CVcontribution_{VCD_{0,GC}} = \frac{\sigma^2_{VCD_{0,GC}}}{\sigma^2_{VCD_{GC}}} \qquad (5a)$$

$$CVcontribution_{dVCD_{Bio,GC}} = \frac{\sigma^2_{dVCD_{Bio,GC}}}{\sigma^2_{VCD_{GC}}} \quad (5b)$$

$$CVcontribution_{dVCD_{Fire,GC}} = \frac{\sigma^2_{dVCD_{Fire,GC}}}{\sigma^2_{VCD_{GC}}} \quad (5c)$$

3. Evaluation on spatial distribution of HCHO VCD and BVOC emissions

Deleted: OMI/OMPS

Deleted: with GEOS-Chem

Figure 1 shows the July mean HCHO VCD over northern high latitudes during 2012-2019, from reprocessed OMI and OMPS-SNPP retrievals, as well as GEOS-Chem model output. We show that OMI and OMPS-SNPP HCHO VCD have consistent spatial patterns and their magnitude agree within 15% (Panel a, b and d). OMPS-SNPP does show lower values in some regions, perhaps due to several cloud and surface reflectance assumptions made in OMPS-SNPP retrievals, or biases that may persist at high-latitudes and large solar zenith angles (Nowlan et al., 2023). While GEOS-Chem well reproduced the spatial pattern of HCHO VCD that OMI and OMPS-SNPP captured (Panel c), we find that GEOS-Chem HCHO VCD is lower than that of OMI by 40%, particularly over wildfire impacted areas (Panel e). The model-satellite discrepancies in wildfire areas can be in part due to model underestimates of VOC emissions and HCHO production from wildfire plumes (Jin et al., 2023), and in part due to the uncertainties in air mass factor calculation for satellite HCHO retrievals in the presence of wildfire smokes (Jung et al., 2019). The model-satellite discrepancies outside wildfire areas could be also due to model underestimates of oxygenated VOCs (OVOCs), biogenic VOC emissions and biases in satellite HCHO retrieval products. For example, Selimovic et al (2022) found that GEOS-Chem underestimates OVOCs, including HCHO, by a factor of 3-12 at Toolik Field Station in Northern Alaska. Stavrakou et al (2015) show model underestimations of biogenic isoprene emission and wildfire emissions over Eastern Europe and Alaska. Recent studies suggest that TROPOMI HCHO retrieval may have a

Deleted: ,

Deleted: and

Deleted: .

Deleted: pattern

Deleted: large

Deleted: associated with

Deleted: can be also due to biases in both model and satellites. For example,

Deleted: attributed the discrepancy at northern high latitudes to low bias in positive bias under low HCHO conditions (Vigouroux et al., 2020). OMPS-SNPP HCHO shows a similar positive bias at clean sites, but has a closer agreement with FTIR HCHO columns at polluted sites (Nowlan et al., 2023; Kwon et al., 2023).

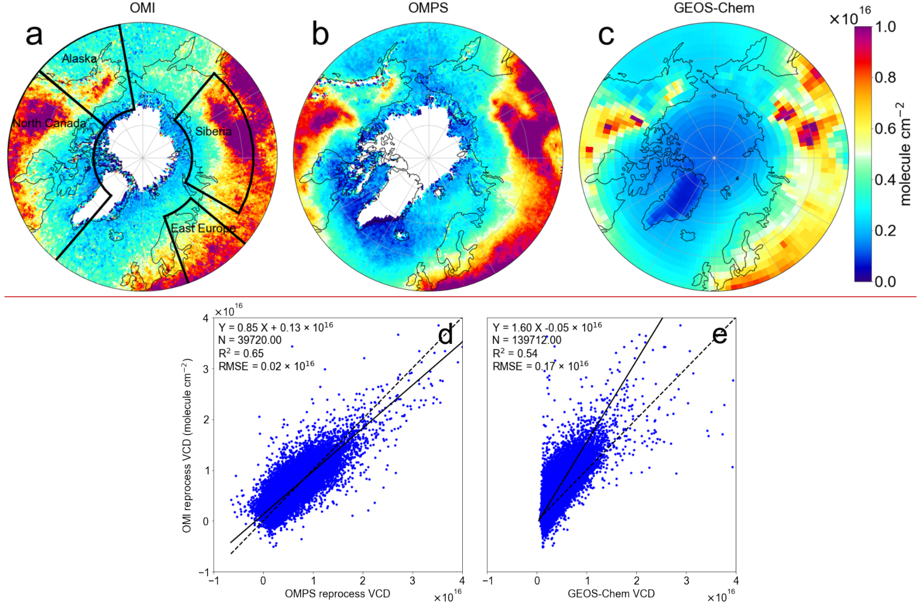

Figure 1. *HCHO VCD from OMI, OMPS-SNPP and GEOS-Chem, as well as their linear correlation.* ***(a)****,* ***(b)*** *and* ***(c)*** *shows Spatial pattern of July mean HCHO VCD from reprocessed OMI, reprocessed OMPS-SNPP and GEOS-Chem over northern high latitudes, in 2012-2019 summers. The black boxes in* ***(a)*** *show the four study domains: Alaska ([50,75] °N, [-170, -130] °E), Siberia ([57,75] °N, [60,140] °E), Northern Canada ([50,75] °N, [-130, -40] °E), Eastern*

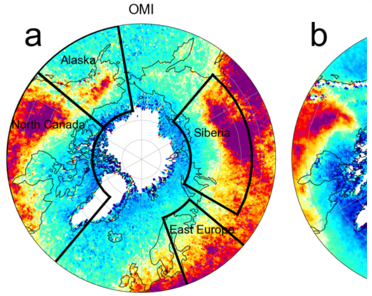

Deleted:

Formatted: Font: Bold

Deleted: |

Deleted: *North*

Deleted: *East*

Europe ([50,71] °N, [20,50] °E). ***(d)*** *Scatter plot of monthly HCHO VCD from reprocessed OMI versus reprocessed OMPS-SNPP over continental northern high latitudes in 2012-2019 summers. OMI and OMPS-SNPP data are regridded to 2° × 2.5° horizontal resolution to matchup with GEOS-Chem pixels.* ***(e)*** *is similar to* ***(d)*** *but shows OMI versus GEOS-Chem.*

We use model sensitivity tests to characterize the spatial variability of HCHO VCD$_{GC,0}$, dVCD$_{Bio,GC}$ and dVCD$_{Fire,GC}$ over northern high latitudes. Figure 2 shows a similar spatial pattern of VCD$_{0,GC}$ and dVCD$_{Bio,GC}$, with a distinctive spatial pattern of dVCD$_{Fire,GC}$. The enhancement of VCD$_{0,GC}$ is mainly shown over Eastern Europe, Eastern Siberia and Central Canada, around 2-4×10^{15} molecules cm^{-2}. dVCD$_{Fire,GC}$ exhibits increases mainly over Alaska, Northern Canada and Central Siberia, with values larger than 5×10^{15} molecules cm^{-2} at fire hot spots. dVCD$_{Bio,GC}$ spatial pattern corresponds mainly to isoprene emissions over vegetated area, enhances over Eastern Europe (2.4×10^{15} molecules cm^{-2}) and Eastern Siberia (1.1×10^{15} molecules cm^{-2}). Model suggests that Eastern Europe is covered by needle leaf evergreen temperate trees and broadleaf deciduous boreal trees, while Eastern Siberia is mainly covered by needle leaf evergreen boreal trees (Figure S1). We note that ΔdVCD$_{Bio,GC}$:ΔISOPe (Isoprene emission flux. Unit: 10^{16} molecules cm^{-2} per 10^{13} atmosC cm^{-2} s^{-1}) over northern high latitudes is around 0.24, a factor of 10 lower than ΔVCD$_{GC}$:ΔISOPe over Southeast US (Millet et al., 2008). This indicates a much lower HCHO production efficiency from isoprene oxidation in northern high latitudes compared to mid-latitude, possibly resulting from the availability of NO$_x$, the difference of temperature, photolysis and oxidants level (Marais et al., 2012; Mao et al., 2013; Li et al., 2016; Wolfe et al., 2016).

Formatted: Font: Italic, English (UK)

Deleted: examine the HCHO VCD along with biogenic and wildfire emissions over Alaska, Siberia, North Canada and East Europe from 2005 to 2019. As shown in Figure 2, both satellites and

Deleted: summertime HCHO VCD over four domains. The interannual variability from both model and satellite, with high HCHO VCD in July, are mainly driven by seasonality of surface temperature, related emissions and chemical production of HCHO. Alaska appears to have the weakest seasonal variation amongst four domains, suggesting a small contribution of biogenic emission in HCHO interannual variability. Consistent with Figure 1, both OMPS-SNPP and OMI HCHO VCDs are higher than modelled values, with largest discrepancies in July. We find from Figure 2 that high HCHO years are often associated with strong wildfire emissions in Alaska, North Canada and Siberia, and to a lesser extent associated with biogenic emissions; while in East Europe, high HCHO years are associated with large biogenic emissions. This indicates different drivers of interannual variabilities of HCHO VCD among these four regions.¶ ... [1]

Moved down [1]: *The blue lines are monthly HCHO VCD*

Deleted: show similar intra-annual and interannual

Deleted: *Red bars are area-normalized wildfire carbon* ... [2]

Moved down [2]: *2.2 and Table S1).*

Deleted: *The R^2 between GEOS-Chem HCHO VCD and* ... [3]

Moved down [3]: 2018; Zhao et al., 2022).

Deleted: Using Mann-Kendall test, we found no significant ... [4]

Deleted: show no significant trend, while the trend of

Deleted: is significant and increasing in Siberia and North ... [5]

Moved down [4]: ¶

Formatted: Font: Bold, English (UK)

Deleted: *3 | Coefficient of Variation (CV) of OMI HCHO* ... [6]

Deleted: VCD$_{0,GC}$ accounts for 66-87% of HCHO VCD in ... [7]

Deleted: shows significant enhancements

Deleted: and North America

Deleted: with high values

Deleted: East

Deleted: 3×10^{15} molecules cm^{-}

Formatted: Not Superscript/ Subscript

Deleted:) and East Siberia (

Deleted:).

Deleted: East

Deleted: East

Deleted: . This indicates a much lower HCHO production ... [8]

Our modelled ISOPe is ~1-2 times higher than MONOe (monoterpenes emission) in Alaska, Europe, Northern Canada and central Siberia boreal forest zone, as shown in Figure 4d and 4e. Our model shows comparable isoprene surface mixing ratios with the in-situ measurements along Trans-Siberian Railway within Russian boreal forests (generally <1ppb in our model, and around 0.31–0.48 ppb in the in-situ campaign in Timkovskys et al (2010), both can reach ~4 ppb in Eastern Siberia). Our model also shows comparable monoterpenes surface mixing ratios over Alaskan North Slope (0.009 ppbv in our model and ~0.014 ppbv in Selimovic et al (2022)). Comparing to Stavrakou et al (2018), our modeled ISOPe over Eastern Europe, Alaska and Northern Canada agrees within 20%, but our modeled MONOe is around 40% lower, likely because we are using online MEGAN, different PFT maps and canopy models (Guenther et al., 2012).

Deleted: North
Deleted: 4(d)
Deleted: (e).
Deleted: can largely reproduce
Formatted: English (UK)
Deleted: East
Deleted: reproduces
Formatted: English (UK)
Formatted: English (UK)
Deleted: East
Deleted: North
Deleted: due to
Deleted: map
Deleted: meteorological fields
Formatted: English (UK)

A remarkable feature is the heterogeneity of BVOC emissions in northern high latitudes revealed by measurements. We show in Table 2 that while isoprene dominates BVOC emission over the Arctic tundra and broadleaf forests, monoterpene becomes the dominated species over coniferous forests. This includes a large portion over European boreal zone, such as at Hyytiälä in Finland (Rinne et al., 2000; Bäck et al., 2012; Rantala et al., 2015; Zhou et al., 2017; Ciarelli et al., 2024), Bílý Kříž in Czech Republic (Juráň et al., 2017) and Norunda research station in Sweden (Wang et al., 2017). However, this large-scale heterogeneity is not being reproduced by our model. We find from Figure 2f that modeled BVOC emissions are dominated by isoprene in most part of northern high latitudes, except Eastern Siberia and East Greenland. As shown in Figure S1, the isoprene-dominated region is mainly due to broad-leaf deciduous boreal shrubs and needle-leaf evergreen boreal trees that are assumed in the model and exhibits higher isoprene emission factors

Deleted: (Rinne et al., 2000; Bäck et al., 2012; Rantala et al., 2015; Zhou et al., 2017), Bílý Kříž in Czech Republic
Formatted: English (UK)
Formatted: English (UK)
Deleted: 4(f)
Deleted: East

than monoterpenes; in contrast, Eastern Siberia is covered predominantly by needle-leaf deciduous boreal trees, leading to higher monoterpenes than isoprene emission (Guenther et al., 2012).

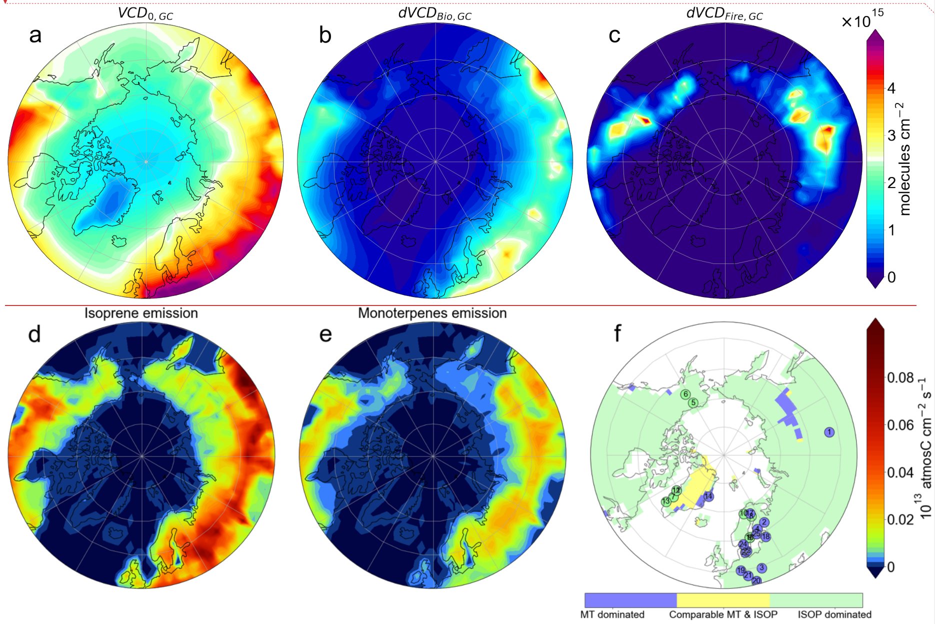

***Figure* 2.** *(a) to (e) GEOS-Chem HCHO $VCD_{0,GC}$, $dVCD_{Bio,GC}$, $dVCD_{Fire,GC}$, isoprene and monoterpenes emission fluxes over northern high latitudes, averaged for July from 2005 to 2019. (f) BVOC emission regimes over northern high latitudes, in GEOS-Chem simulation for 2005-2019 summers and from in-situ measurements (references listed in Table 2). Isoprene-dominates regime at a pixel means isoprene emission is significantly higher than monoterpenes emission ($p<0.05$ in t-test) for May-August in 2005-2019.*

Deleted: East

Formatted: English (UK)

Deleted: . We expect the discrepancy between model and measurement to have small effects on HCHO VCD, as BVOC generally contributes to less than 9-37% of HCHO VCD in high HCHO years and 12-27% in low HCHO years.

Deleted: ¶

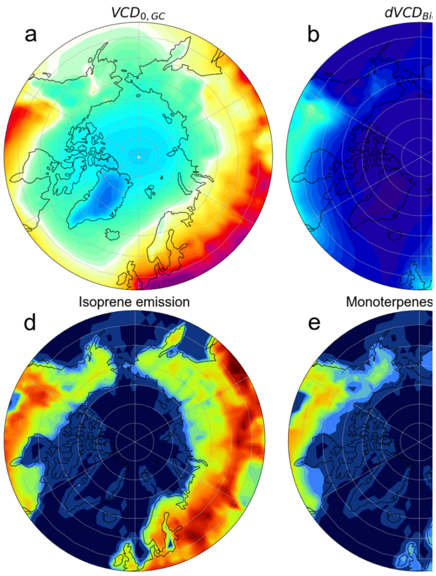

Formatted: Font: Bold

Deleted: *4*

Table 2. In-situ measurements of BVOC in Figure 2f

Site name	**Lat(°N), Lon(°E)**	**Period of the measurement**	**Major vegetation type at location of measurement**	**Predominant BVOC**	**References**
[1] Irkutsk	53.00, 102.27	July 21 to August 4 2008	Boreal coniferous forest	Monoterpenes*	Timkovsky et al., 2010
[2] Pötsönvaara	62.72, 30.96	May to October 1997-1998	mixed forest	Monoterpenes*	Hakola et al., 2000
[3] Bílý Kříž	49.50, 18.54	Summer 2009-2014	Norway spruce forest	Monoterpenes	Juráň et al., 2017
[4] Hyytiälä	61.84, 24.29	1) August 2001 2) May, 2010 to December 2013 3) April to November 2008 4) April 2000 to April 2002	Boreal coniferous forest (Scots pine (Pinus sylvestris) and Norway spruce (Picea abies))	Monoterpenes	Spirig et al., 2004, Rantala et al., 2015 (emission),

Formatted: Justified
Deleted: 4(f)
Formatted: Font: 12 pt
Formatted Table
Formatted: Font: 12 pt
Formatted: Justified
Deleted: –
Formatted: Font: 12 pt
Formatted: Font: 12 pt
Deleted: ,
Formatted: Font: 12 pt
Deleted: ,
Formatted: Font: 12 pt
Formatted: Font: 12 pt
Formatted: Font: 12 pt
Deleted: Pitkälahti
Formatted: Font: 12 pt
Formatted: Justified
Formatted: Font: 12 pt
Formatted: Justified
Deleted: ,
Formatted: Font: 12 pt
Formatted: Font: 12 pt
Formatted: Justified
Formatted: Font: 12 pt
Formatted: Font: 12 pt
Formatted: Justified
Deleted: ,
Formatted: Font: 12 pt
Formatted: Font: 12 pt, Spanish (Traditional Sort)
Formatted: Font: 12 pt
Deleted: ,
Formatted: Font: 12 pt
Formatted: Font: 12 pt
Deleted: ,
Formatted: Justified
Formatted: Font: 12 pt

					Aaltonen et al., 2011 (emission), Hakola et al., 2003,
[5] TFS	68.63, -149.59	May to June 2019	Arctic Tundra	Isoprene	Angot et al., 2020; Selimovic et al., 2022
[6] Fairbanks	64.84, -147.72	August 2016	Needle-leaf evergreen boreal forest	Isoprene*	Zhao et al., 2022
[7]Kangerlussuaq	67.01, -50.73	late June to early August 2013	Salix spp.	Isoprene	Vedel-Petersen et al., 2015
[8] Lompolojänkkä	66.61, 24.06	May to August 2018	Sub-Arctic fen	Isoprene, Monoterpenes*	Hellén et al., 2020
[9] NOPEX site	60.08, 17.50	May to September 1995	mixed forest	Isoprene	Janson et al., 1999

Formatted: Font: 12 pt
Formatted: Font: 12 pt, Finnish
Formatted: Justified
Formatted: Font: 12 pt
Formatted: Font: 12 pt
Formatted: Justified
Deleted: –
Formatted: Font: 12 pt
Formatted: Font: 12 pt
Formatted: Font: 12 pt
Formatted: Justified
Formatted: Font: 12 pt
Formatted: Font: 12 pt
Formatted: Font: 12 pt
Formatted: Font: 12 pt
Formatted: Justified
Formatted: Font: 12 pt
Deleted: (Salix spp.)
Formatted: Font: 12 pt
Formatted: Font: 12 pt
Formatted: Font: 12 pt
Formatted: Justified
Deleted: ,
Formatted: Font: 12 pt
Formatted: Font: 12 pt
Formatted: Justified
Formatted: Font: 12 pt
Formatted: Font: 12 pt
Formatted: Font: 12 pt
Formatted: Font: 12 pt
Formatted: Justified
Deleted: ,
Formatted: Font: 12 pt
Formatted: Font: 12 pt

[10] Abisko Scientific Research Station	68.35, 18.82	June to August 2006-2007,2010-2012	Subarctic wet heath	Isoprene	Tiiva et al., 2008; Faubert et al., 2010; Valolahti et al., 2015
[11] Disko	69.24, - 53.53	June to August 2013-2014	Subarctic heath	Monoterpenes	(Lindwall et al., 2016a)
[12] Disko	69.24, - 53.53	June to August 2014-2015	Arctic fen	Isoprene	(Lindwall et al., 2016b)
[13] Nuuk	64.12, - 51.35	June to August 2013	Subarctic heath	Isoprene	Kramshøj et al., 2016
[14] Zackenberg	74.50, - 20.50	August 2009	Mesic to dry mixed heath	Monoterpenes	Schollert et al., 2014
[15] Norunda	60.08, 17.48	June to September 2013	Dominated by 80-123-years old Norway spruce and Scots pine	Monoterpenes	Wang et al., 2017

Deleted: ,
Formatted: Font: 12 pt
Formatted: Font: 12 pt
Formatted: Font: 12 pt
Formatted: Justified
Formatted: Font: 12 pt
Formatted: Justified
Deleted: ,
Formatted: Font: 12 pt
Formatted: Font: 12 pt
Formatted: Font: 12 pt
Formatted: Font: 12 pt
Formatted: Font: 12 pt
Formatted: Justified
Deleted: ,
Formatted: Font: 12 pt
Formatted: Font: 12 pt
Formatted: Font: 12 pt
Formatted: Font: 12 pt
Formatted: Justified
Deleted: ,
Formatted: Font: 12 pt
Formatted: Font: 12 pt
Formatted: Justified
Deleted: ,
Formatted: Font: 12 pt
Formatted: Font: 12 pt
Deleted: (
Deleted:)
Formatted: Font: 12 pt
Formatted: Justified
Formatted: Font: 12 pt
Deleted: (
Formatted: Font: 12 pt
Deleted: ,
Formatted: Font: 12 pt
Deleted:)
Formatted: Font: 12 pt
Moved down [5]: Norway Spruce
Formatted: Font: 12 pt

[16] Norunda	60.08, 17.48	June to July 2014	Dominated by 80-123-years old Norway spruce and Scots pine	Isoprene	(van Meeningen et al., 2017)
[17] Pallas Kenttärova	67.59, 24.15	April to August, 2020	Norway Spruce	Sesquiterpenes, Monoterpenes	Hakola et al., 2023
[18] Järvselja, Estonia	58.27, 27.27	26 September to 17 October 2012	Norway spruce	Monoterpenes	(Bourtsoukidis et al., 2014b)
[19] Taunus Observatory, Germany	50.22, 8.43	8 April to 11 November 2011	Norway Spruce	Monoterpenes	(Bourtsoukidis et al., 2014a)
[20] Ljubljana, Slovenia	46.07, 14.50	April to May 2016	Norway spruce	Monoterpenes	(van Meeningen et al., 2017)
[21] Grafrath, Germany	48.30, 11.28	June 2014, 2016	Norway spruce	Monoterpenes	(van Meeningen et al., 2017)

Moved (insertion) [5]

[22] Taastrup, Denmark	55.67, 12.30	July to August 2013, July 2014-2016	Norway spruce	Monoterpenes	(van Meeningen et al., 2017)
[23] Hyltemossa, Sweden	56.10, 13.42	July 2016	Norway spruce with a small fraction of Downy birch and Scots pine	Monoterpenes	(van Meeningen et al., 2017)
[24] Skogaryd, Sweden	58.38, 12.15	October 2015	coniferous trees, dominated by Norway spruce and Scots Pine	Monoterpenes	(van Meeningen et al., 2017)
[25] Piikkiö, Finland	60.38, 22.50	July to August, 2014	Norway spruce	Monoterpenes	(van Meeningen et al., 2017)

For the column ‘Predominant BVOC’, with * means ‘Most abundant BVOC in mixing ratio’, without * means ‘Most emitted BVOC’.

Deleted: ¶
Figure 5(a) to (c) shows that wildfire is the main driver of HCHO VCD interannual variability over Siberia, north Canada and Alaska. In low HCHO years of these three domains, $dVCD_{Fire,GC}$ contribution ~5-10

4. Examination on the interannual variabilities of HCHO VCD

Figure 3 shows that in Alaska, Northern Canada and Siberia, high HCHO years are often associated with strong wildfire VOC emissions (R^2=0.78-0.89) and to a lesser extent associated with biogenic VOC emissions (R^2=0.21-0.47). The interannual variability of wildfire VOC emission is further supported by CO emissions from both GFED4 and satellite-based estimation (Yurganov and Rakitin, 2022). The high correlation between OMI HCHO VCD and GFED wildfire VOC emissions in Alaska, Siberia and Northern Canada indicates a strong wildfire impact on interannual variabilities of HCHO VCD in these domains. In Eastern Europe, high HCHO years are associated with large biogenic emissions (With wildfire VOC emissions: R^2=0.51; With biogenic emissions: R^2=0.72), indicating the important role of biogenic emission in interannual variability of HCHO in Eastern Europe.

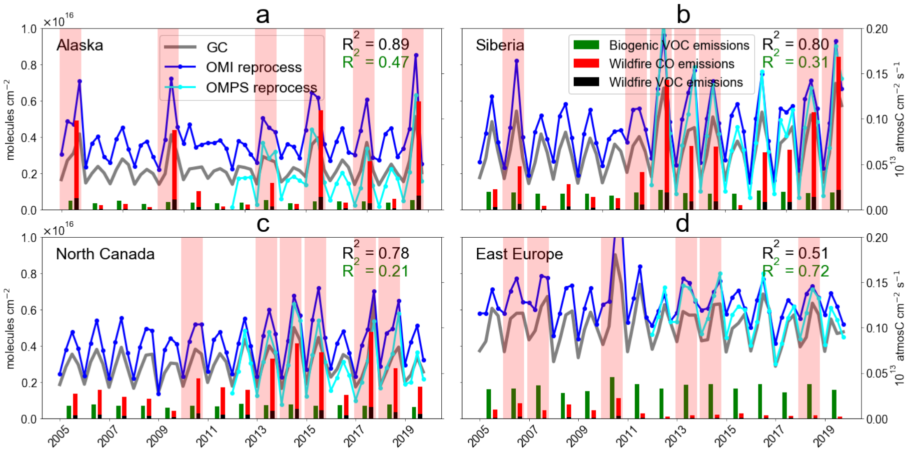

Figure 3. *Timeseries of HCHO VCD, biogenic and wildfire emissions over (a) Alaska, (b) Siberia, (c) Northern Canada and (d) Eastern Europe, May 1-August 31, 2005-2019. The blue lines are monthly HCHO VCD from reprocessed OMI, cyan lines are from reprocessed OMPS-SNPP, grey*

Moved (insertion) [1]

lines are from GEOS-Chem. Red and black bars are area-normalized wildfire CO and VOC emissions during the summer of each year; green bars are area-normalized biogenic VOC emissions. Wildfire emissions are calculated from GFED4.1s inventory; biogenic VOC emissions are calculated by MEGAN2.1 model. Pink shade indicates high HCHO VCD years (definition see Sect. 2.2 and Table S1). The R^2 between reprocessed OMI HCHO VCD and biogenic VOC emission (green) / wildfire VOC emission (black) is shown at top right of each panel.

Figure 4a to 4c shows that wildfire is the main driver of HCHO VCD_{GC} interannual variability over Siberia, Northern Canada and Alaska. In low HCHO years of these three domains, $dVCD_{Fire,GC}$ contribution ~2-11% of HCHO total column, less than $VCD_{0,GC}$ and $dVCD_{Bio,GC}$; in high HCHO years, $dVCD_{Fire,GC}$ contribution to total column rises to ~20-34%. This is consistent with Figure 3 that HCHO VCD interannual variability have significantly higher correlations with wildfire emissions (R^2=0.78-0.89) than with biogenic emission (R^2=0.21-0.47) over Siberia, Northern Canada and Alaska. These findings highlight the role of wildfire in driving HCHO interannual variability in the three domains.

In Eastern Europe, biogenic emission and background HCHO accounts for the majority of HCHO VCD interannual variability, largely due to the relatively higher surface temperature, stronger photolysis, higher oxidants level and higher availability of NO_x than the other three domains. In regional scale, BVOC emissions and methane oxidation with hydroxyl radicals (OH) both depend on temperature (Guenther et al., 2012; Holmes et al., 2013). In Figure 4d, the surface temperature in Eastern Europe is higher than that in Alaska, Northern Canada and Siberia by 5-7 K, leading to an increase in BVOC emissions and $VCD_{0,GC}$ through methane oxidation. HCHO VCD is further

Moved (insertion) [2]

Deleted: 40

Deleted: 2

Deleted: north

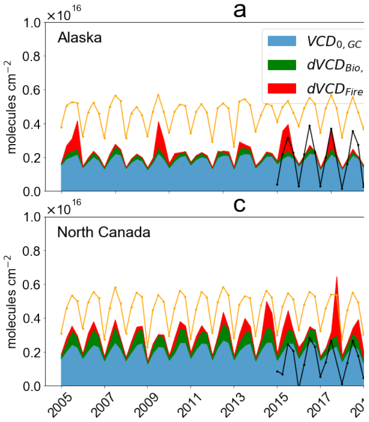

Deleted:
¶
Figure 5 | Interannual variability of monthly HCHO $VCD_{0,GC}$, $dVCD_{Bio,GC}$ and $dVCD_{Fire,GC}$ as well as near-surface temperature over (a) Alaska, (b) Siberia, (c) North Canada and (d)East Europe, in 2005-2019 summers.

Moved down [6]: *The indigo, green and red shades are background HCHO $VCD_{0,GC}$, $dVCD_{Bio,GC}$ and $dVCD_{Fire,GC}$, based on GEOS-Chem sensitivity tests (Table 1). The orange curves are monthly surface temperature from MERRA-2 dataset. The black curves are OCO-2 monthly SIF.*¶
¶

Deleted: In East Europe, biogenic emission and background HCHO accounts for the majority of HCHO VCD interannual variability, largely due to surface temperature and availability of NO_x. In Figure 5(d), the surface temperature in East Europe is higher than that in Alaska, North enhanced through the higher NO_x level (0.4-1ppbv) in Eastern Europe than in other three domains (0.1-0.5ppbv), as HCHO yield from isoprene photooxidation increases with NO_x level. The high NO_x level in Eastern Europe results from its large urban areas and high anthropogenic emissions. The large contribution of BVOC to HCHO VCD is consistent with Figure 5, which shows the CV of $dVCD_{Bio,GC}+VCD_{0,GC}$ accounts >90% of VCD_{GC}'s CV in Eastern Europe. Similarly, Figure 3d shows that biogenic emission has a higher correlation (R^2 = 0.72) with VCD_{GC} than wildfire emission does (R^2=0.51). These results suggest that biogenic emission and background are the main contributors of HCHO interannual variability in Eastern Europe.

Deleted: East

Deleted: East

Deleted: 3

Deleted: East

Deleted: 2(d)

Deleted: 87

Deleted: 24

Deleted: East

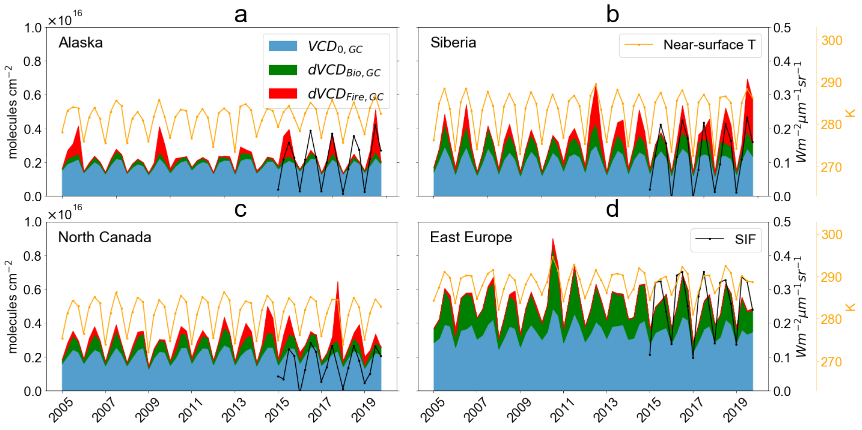

Moved (insertion) [4]

Formatted: Justified

Formatted: Font: Bold, English (UK)

Figure 4*. Interannual variability of monthly HCHO $VCD_{0,GC}$, $dVCD_{Bio,GC}$ and $dVCD_{Fire,GC}$ as well as near-surface temperature over (a) Alaska, (b) Siberia, (c) Northern Canada and (d) Eastern Europe, in 2005-2019 summers. In each year, only the monthly values in May, June, July and August are shown. The indigo, green and red shades are background HCHO $VCD_{0,GC}$, $dVCD_{Bio,GC}$*

Moved (insertion) [6]

and dVCD$_{Fire,GC}$, based on GEOS-Chem sensitivity tests (Table 1). The orange curves are monthly surface temperature from MERRA-2 dataset. The black curves are OCO-2 monthly SIF.

We further examine the contribution from background, biogenic and pyrogenic emissions to the interannual variability of HCHO VCD$_{GC}$ over each region. We find from model results that biogenic emission and background signal contributes to 90% of the interannual variability of HCHO VCD$_{GC}$ in Eastern Europe, while wildfire accounts for over 90% of CV in Alaska, Siberia and Northern Canada, consistent with previous work (Stavrakou et al., 2018; Zhao et al., 2022). We use Mann-Kendall test, a non-parametric statistical test used to detect trends in time series data, to test the significance of the trend of monthly HCHO VCD$_{GC}$ time series over a specific domain (Gilbert, 1987). We found no significant trend of HCHO VCD$_{GC}$ over Eastern Europe, Northern Canada and Alaska from either satellites or model. On the other hand, we find the trend of HCHO VCD$_{GC}$ over Siberia is significant ($p<0.05$) and increasing (1.7% per year). VCD$_{0,GC}$ and dVCD$_{Bio,GC}$ show no significant trend, while the trend of dVCD$_{Fire,GC}$ is significant and increasing in Siberia (12% per year), suggesting that wildfires are responsible for the VCD$_{GC}$ trends in Siberia. In contrast to Bauwens et al (2016), We find that HCHO VCD$_{GC}$ trend over Siberia is largely driven by the increasing wildfires in recent years, and to a lesser extent by biogenic VOC emissions, highlighting the important role of wildfires on HCHO VCD interannual variability.

Formatted: Justified

Moved (insertion) [3]

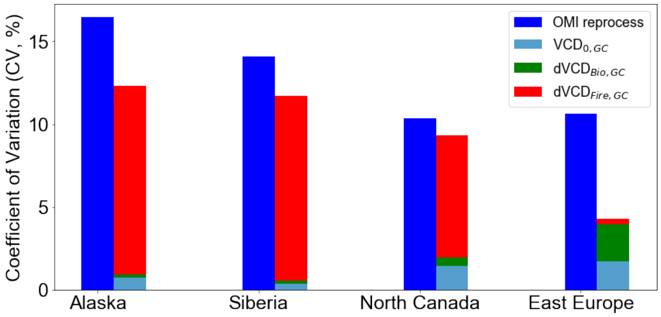

Figure 5. *Coefficient of Variation (CV) of OMI HCHO VCD, modelled HCHO $VCD_{0,GC}$, $dVCD_{Bio,GC}$ and $dVCD_{Fire,GC}$ in summertime of 2005-2019.*

5. SIF evaluation on $dVCD_{Bio,GC}$ interannual variability

In Figure 6a to 6d, we find a good linear relationship (R=0.6-0.7) between OCO-2 monthly SIF and $dVCD_{Bio,GC}$ at Alaska, Siberia, Northern Canada and Eastern Europe. Foster et al (2014) show a high linear correlation between seasonal variation of satellite HCHO column (fire free) and GPP in northern high latitudes. This is consistent with our finding over most continental areas in northern high latitudes (Figure S2), since SIF is a widely used proxy of GPP (Frankenberg et al., 2011). In Figure 6g to 6j, SIF and ISOPe show a linear relationship when SIF is within 0-0.25 $Wm^{-2}\mu m^{-1}sr^{-1}$ but tend to decouple when SIF > 0.25 $Wm^{-2}\mu m^{-1}sr^{-1}$, possibly due to the different temperature optimums of isoprene emission and photosynthesis (Harrison et al., 2013; Zheng et al., 2015).

Despite the difference in distribution of vegetation types, the $dVCD_{Bio,GC}$-SIF slope is homogeneous over Siberia, Northern Canada and Eastern Europe (slope=0.28-0.45, unit:10^{16}

Deleted: To further evaluate the drivers of interannual variability of HCHO VCD, we examine the correlation between SIF and HCHO signal from various regions. In Figure 6, SIF and $dVCD_{Bio,GC}$ or ISOPe show better coupling under a lower SIF level

Moved down [7]: , possibly due to the different temperature optimums of isoprene emission and photosynthesis (Harrison et al., 2013; Zheng et al., 2015).

Deleted: We calculated the correlation via Standardized Major Axis (SMA) regression for SIF within 0-0.25 $Wm^{-2}\mu m^{-1}sr^{-1}$. Figure 6(a)-(d) show a similar linear regression slope between SIF and $dVCD_{Bio,GC}$ over the East Europe, Siberia and North Canada, a factor of 3-4 higher than the slope over Alaska. The good correlation between SIF and $dVCD_{Bio,GC}$ is expected, as both are largely driven by surface temperature (Figure S2 and S3) . Despite the difference in distribution of vegetation types, the similar $dVCD_{Bio,GC}$-SIF slopes over Siberia, North Canada and East Europe (slope=0.27-0.43, unit:10^{16} molecules cm^{-2} per $Wm^{-2}\mu m^{-1}sr^{-1}$), indicates SIF as a proxy of $dVCD_{Bio,GC}$ spatiotemporal variability in these domains. The low $dVCD_{Bio,GC}$-SIF slope in Alaska warrants further investigation. ¶
¶
We further examine the relationship between ISOPe and SIF. We find ISOPe:SIF slopes to be less uniform compared to $dVCD_{Bio,GC}$-SIF slopes, likely due to the widespread enhancement of HCHO VCD that largely reduces the spatial gradient of isoprene emissions (Zhao et al. 2022). In contrast to high latitudes, we find that both ISOPe:SIF slope and $dVCD_{Bio,GC}$:SIF slope are significantly higher in Southeast US and Amazon (Figure 6(e)-(f), (k)-(l)), suggesting much stronger isoprene emissions per unit of SIF at lower latitudes.…

Formatted: English (UK)

Deleted: to

Deleted: that $dVCD_{Bio,GC}$ and SIF are highly correlated

Moved (insertion) [7]

Formatted: English (UK)

molecules cm^{-2} per Wm^{-2}μm^{-1}sr^{-1}), suggesting SIF as a tool to understand biogenic HCHO variability in these regions. The dVCD$_{Bio,GC}$-SIF slope in Alaska is 3-5 times lower than other three domains, which warrants further investigation. In contrast to high latitudes, we find that both ISOPe:SIF slope and dVCD$_{Bio,GC}$:SIF slope are a factor of 2-10 times higher in Southeast US and Amazon (Figure 6e-6f, 6k-6l) than in northern high latitudes, indicating that the dVCD$_{Bio,GC}$-SIF slope over northern high latitudes and lower latitudes could be very different.

SIF offers an independent evaluation on the interannual variability of HCHO dVCD$_{Bio,GC}$. As SIF showing a linear relationship with dVCD$_{Bio,GC}$ in northern high latitudes (Figure 6a to 6d), it is reasonable to infer from Figure 4 that the low interannual variability shown in SIF (CV=1-9%) is expected for dVCD$_{Bio,GC}$ (CV=1-2%) in Alaska, Siberia and Northern Canada. In contrast, we find that dVCD$_{Fire,GC}$ has a much weaker correlation with SIF (Figure S2c) and shows a higher interannual variability (CV=8-13%). As wildfire emission is highly correlated (R^2=78-89%) with OMI HCHO VCD over Northern Canada, Siberia, and Alaska (Figure 3), the high interannual variabilities of OMI HCHO VCD (CV=10-16%) in these domains are likely driven by wildfires instead of biogenic emissions.

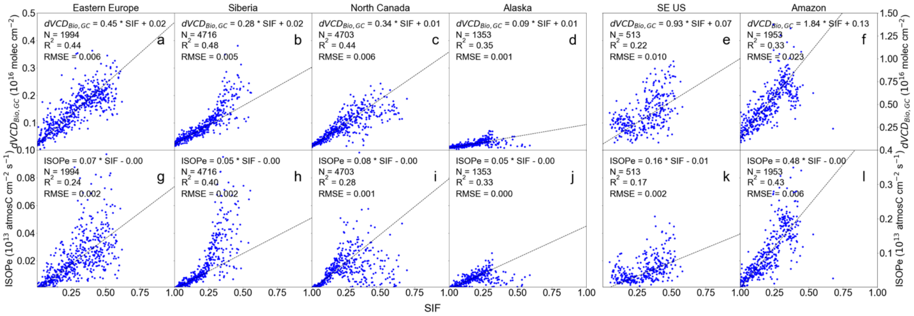

Deleted: BVOC emissions

Deleted: are tightly correlated

Deleted: and isoprene emissions,

Deleted: 5

Formatted: English (US)

Deleted: isoprene emissions in four domains.

Deleted: between

Formatted: English (US)

Deleted: dVCD$_{Fire,GC}$, suggesting that the low

Deleted: of SIF cannot be applied to wildfire emissions and their contribution to HCHO VCD.

Deleted: interannual variability

Deleted: North

Deleted: 2), it is unlikely that

Deleted: strong HCHO

Deleted:

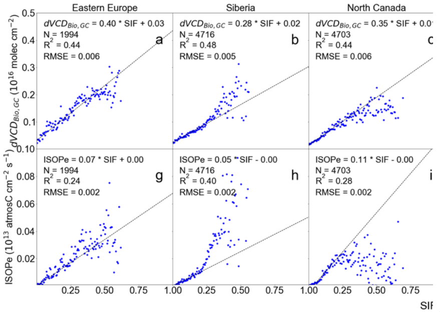

Figure 6 *. Scatter plot of monthly OCO-2 SIF versus GEOS-Chem HCHO* $dVCD_{Bio,GC}$ *and isoprene emission fluxes in the four study domains plus Southeast US ([26, 36]°N, [-100,-75]°E) and Amazon([-20,-5]°N, [-75,-40]°E), from May to August in 2015-2019. OCO-2 SIF is regridded to 2° × 2.5° spatial resolution. Only continental pixels of SIF-*$dVCD_{Bio,GC}$ *and SIF-ISOPe matchups are used to plot. Before plotting, data matchups are binned by SIF, using a bin size of 0.001* $Wm^{-2}\mu m^{-1}sr^{-1}$*. Linear regression is shown as the black dash in each panel, calculated for SIF within 0-0.25* $Wm^{-2}\mu m^{-1}sr^{-1}$*. Amount of binned data pairs (N), R-Squared (*R^2*), Root Mean Square Error (RMSE) are calculated based on binned data across all ranges.*

Formatted: Font: Bold

Formatted: Left

Deleted: |

Deleted: *005*

Deleted: *SMA*

Formatted: English (US)

6. Conclusions and discussions

We use reprocessed new retrievals of HCHO from OMI and OMPS-SNPP to evaluate the interannual variability of HCHO VCD from GEOS-Chem over northern high latitudes in 2005-2019 summers. The reprocessed OMI and OMPS-SNPP HCHO VCDs show a high consistency in the spatial pattern and interannual variability. GEOS-Chem reproduced the interannual variability of HCHO VCD but the magnitude is biased low comparing to satellite retrievals.

Our modeled HCHO VCD can be biased low, due to large underestimate of HCHO production and emission factor in wildfire smokes. Previous in-situ campaigns show underestimated emission factors of VOCs in GFED4.1s emission inventory for temperate forests in western US (Liu et al., 2017; Permar et al., 2021), while the bias in VOC emission factor in boreal forest wildfires remains unclear. HCHO underestimation can also be due to the missing HCHO secondary production in wildfire-impacted conditions (Liao et al., 2021; Jin et al., 2023). GEOS-Chem is found to underestimate oxygenated VOCs by a factor of 3 to 12 in some Arctic regions, which could contributes to the bias in modelled HCHO in northern high latitudes (Selimovic et al., 2022). More measurements in Arctic region are needed to reconcile the model-observation discrepancies.

Wildfire accounts for the majority of HCHO interannual variability in Alaska, Northern Canada and Siberia. Compared to biogenic emissions and background HCHO, wildfire emission shows a better correlation with HCHO VCD, despite that biogenic and background HCHO can dominate HCHO VCD in low HCHO years of these three regions. We also find an increasing trend ($p < 0.05$) in wildfire emission and HCHO VCD over Northern Canada and Siberia. With rapid Arctic warming, wildfire frequency and intensity rises rapidly in recent decades and near future (Descals et al., 2022). We expect wildfire continues to dominate HCHO interannual variability in the three regions.

Eastern Europe is the only one of the four studied regions where HCHO interannual variability is dominated by biogenic emission and background HCHO. This is due to a combination of lower wildfire activities, higher surface temperature and anthropogenic NO_x emissions in this region. No significant trend of biogenic emission, biogenic-related HCHO and background HCHO are found in the four regions during summertime of 2005-2019. However, model estimate of HCHO from biogenic emissions are largely uncertain, as model calculated VOC speciation is at odds with field measurements (Figure 2f and Table 2). Previous work shows good performance of model in capturing long-term variability of biogenic emission in response to climate variables (Stavrakou et al., 2018), but model underestimates biogenic and fire emissions over northern high latitudes,

Deleted: North

Deleted: North Canada and Siberia. In fact, our modeled HCHO VCD can be biased low, due to large underestimate of HCHO from wildfire emissions (Liao et al., 2021; Liu et al., 2017; Permar et al., 2021).

Deleted: East

Deleted: 4(f)

especially over Eastern Europe and Alaska (Stavrakou et al., 2015). Future research is warranted to examine the HCHO signal from biogenic emissions in this region.

Deleted: East

The OCO-2 satellite SIF provides an additional constraint on the interannual variability of biogenic emissions and is independent of wildfire emissions. As a proxy of vegetation photosynthesis and GPP, SIF is expected to have a good correlation with isoprene emission and HCHO VCD in the northern boreal regions, though this correlation can be worse in mid-latitudes and tropical region (Foster et al., 2014). We show a tight and homogeneous linear relationship (R=0.6-0.7) between SIF and dVCD$_{\mathrm{Bio,GC}}$ at northern high latitudes, suggesting that SIF may serve as a tool to understand biogenic HCHO variability in this region.

Deleted: correlation

Deleted: , and between SIF and isoprene emissions

Deleted: can be used as a proxy for isoprene emissions in this region. It remains unclear why the dVCD$_{\mathrm{Bio,GC}}$-SIF slope in Alaska is lower than other domains. SIF

Deleted: emissions at northern high latitudes

Code and data availability.

The OMPS-SNPP HCHO L2 V1 product is available at https://disc.gsfc.nasa.gov/datasets/OMPS_NPP_NMHCHO_L2_1/summary (González Abad, 2022). The OMI HCHO L2 product is available at https://waps.cfa.harvard.edu/sao_atmos/data/omi_hcho/OMI-HCHO-L2/ . The OCO-2 SIF is available at https://daac.ornl.gov/cgi-bin/dsviewer.pl?ds_id=1863 (Yu et al., 2021). Data used in this work is available at https://doi.org/10.6084/m9.figshare.23599566.v1 (Zhao, 2023a). Data processing and plotting codes are available at https://doi.org/10.5281/zenodo.8094844 (Zhao, 2023b). The GEOS-Chem model is publicly available at: https://doi.org/10.5281/zenodo.3701669 (GEOS-Chem, 2020).

Deleted: (xxxxx).

Deleted:

Supplement.

The supplement related to this article is available online at: https://doi.org/10.6084/m9.figshare.25130813.v1 .

Deleted: (xxxxx).

Author contributions.

TZ and JM designed the research, performed the simulations and conducted the analysis. ZA, GGA and CN provided OMI and OMPS data. YZ helped process and analyze the data. TZ and JM wrote the paper with all co-authors providing input.

Competing interests.

The contact author has declared that neither they nor their co-authors have any competing interests.

Disclaimer.

Acknowledgement.

TZ and JM acknowledge funding from NASA grant 80NSSC19M0154 and 80NSSC21K0428. ZA, GGA and CN acknowledge funding from NOAA grant NA18OAR4310108 and NASA grants 80NSSC18M0091, 80NSSC18K0691 and 80NSSC21K0177. We thank William Simpson (University of Alaska Fairbanks) for helpful discussions.

References

Aaltonen, H., Pumpanen, J., Pihlatie, M., Hakola, H., Hellén, H., Kulmala, L., Vesala, T., and Bäck, J.: Boreal pine forest floor biogenic volatile organic compound emissions peak in early summer and autumn, Agricultural and Forest Meteorology, 151, 682–691, https://doi.org/10.1016/j.agrformet.2010.12.010, 2011.

Formatted: Line spacing: single

Affek, H. P. and Yakir, D.: Natural Abundance Carbon Isotope Composition of Isoprene Reflects Incomplete Coupling between Isoprene Synthesis and Photosynthetic Carbon Flow, Plant Physiology, 131, 1727–1736, https://doi.org/10.1104/pp.102.012294, 2003.

Akagi, S. K., Yokelson, R. J., Wiedinmyer, C., Alvarado, M. J., Reid, J. S., Karl, T., Crounse, J. D., and Wennberg, P. O.: Emission factors for open and domestic biomass burning for use in atmospheric models, Atmospheric Chemistry and Physics, 11, 4039–4072, https://doi.org/10.5194/acp-11-4039-2011, 2011.

Alvarado, L. M. A., Richter, A., Vrekoussis, M., Hilboll, A., Kalisz Hedegaard, A. B., Schneising, O., and Burrows, J. P.: Unexpected long-range transport of glyoxal and formaldehyde observed from the Copernicus Sentinel-5 Precursor satellite during the 2018 Canadian wildfires, Atmospheric Chemistry and Physics, 20, 2057–2072, https://doi.org/10.5194/acp-20-2057-2020, 2020.

Formatted: Line spacing: single

Angot, H., McErlean, K., Hu, L., Millet, D. B., Hueber, J., Cui, K., Moss, J., Wielgasz, C., Milligan, T., Ketcherside, D., Bret-Harte, M. S., and Helmig, D.: Biogenic volatile organic compound ambient mixing ratios and emission rates in the Alaskan Arctic tundra, Biogeosciences Discussions, 1–39, https://doi.org/10.5194/bg-2020-235, 2020.

Atkinson, R.: Atmospheric chemistry of VOCs and NOx, Atmospheric Environment, 34, 2063–2101, https://doi.org/10.1016/S1352-2310(99)00460-4, 2000.

Bäck, J., Aalto, J., Henriksson, M., Hakola, H., He, Q., and Boy, M.: Chemodiversity of a Scots pine stand and implications for terpene air concentrations, Biogeosciences, 9, 689–702, https://doi.org/10.5194/bg-9-689-2012, 2012.

Formatted: Line spacing: single

Bauwens, M., Stavrakou, T., Müller, J. F., De Smedt, I., Van Roozendael, M., van der Werf, G. R., Wiedinmyer, C., Kaiser, J. W., Sindelarova, K., and Guenther, A.: Nine years of global hydrocarbon emissions based on source inversion of OMI formaldehyde observations, Atmos. Chem. Phys., 16, 10133–10158, https://doi.org/10.5194/acp-16-10133-2016, 2016.

Bindle, L., Martin, R. V., Cooper, M. J., Lundgren, E. W., Eastham, S. D., Auer, B. M., Clune, T. L., Weng, H., Lin, J., Murray, L. T., Meng, J., Keller, C. A., Putman, W. M., Pawson, S., and Jacob, D. J.: Grid-stretching capability for the GEOS-Chem 13.0.0 atmospheric chemistry model, Geoscientific Model Development, 14, 5977–5997, https://doi.org/10.5194/gmd-14-5977-2021, 2021.

Blake, D. R., Hurst, D. F., Smith, T. W., Whipple, W. J., Chen, T.-Y., Blake, N. J., and Rowland, F. S.: Summertime measurements of selected nonmethane hydrocarbons in the Arctic and

Subarctic during the 1988 Arctic Boundary Layer Expedition (ABLE 3A), J. Geophys. Res., 97, 16559, https://doi.org/10.1029/92JD00892, 1992.

Boeke, N. L., Marshall, J. D., Alvarez, S., Chance, K. V., Fried, A., Kurosu, T. P., Rappenglück, B., Richter, D., Walega, J., Weibring, P., and Millet, D. B.: Formaldehyde columns from the Ozone Monitoring Instrument: Urban versus background levels and evaluation using aircraft data and a global model, J. Geophys. Res., 116, D05303, https://doi.org/10.1029/2010JD014870, 2011.

Bourtsoukidis, E., Williams, J., Kesselmeier, J., Jacobi, S., and Bonn, B.: From emissions to ambient mixing ratios: online seasonal field measurements of volatile organic compounds over a Norway spruce-dominated forest in central Germany, Atmospheric Chemistry and Physics, 14, 6495–6510, https://doi.org/10.5194/acp-14-6495-2014, 2014a.

Bourtsoukidis, E., Bonn, B., and Noe, S. M.: On-line field measurements of BVOC emissions from Norway spruce (Picea abies) at the hemiboreal SMEAR-Estonia site under autumn conditions, Boreal Environment Research, 2014b.

Ciarelli, G., Tahvonen, S., Cholakian, A., Bettineschi, M., Vitali, B., Petäjä, T., and Bianchi, F.: On the formation of biogenic secondary organic aerosol in chemical transport models: an evaluation of the WRF-CHIMERE (v2020r2) model with a focus over the Finnish boreal forest, Geoscientific Model Development, 17, 545–565, https://doi.org/10.5194/gmd-17-545-2024, 2024.

Delwiche, C. F. and Sharkey, T. D.: Rapid appearance of 13C in biogenic isoprene when 13CO2 is fed to intact leaves, Plant, Cell & Environment, 16, 587–591, https://doi.org/10.1111/j.1365-3040.1993.tb00907.x, 1993.

Descals, A., Gaveau, D. L. A., Verger, A., Sheil, D., Naito, D., and Peñuelas, J.: Unprecedented fire activity above the Arctic Circle linked to rising temperatures, Science, 378, 532–537, https://doi.org/10.1126/science.abn9768, 2022.

Eastham, S. D., Long, M. S., Keller, C. A., Lundgren, E., Yantosca, R. M., Zhuang, J., Li, C., Lee, C. J., Yannetti, M., Auer, B. M., Clune, T. L., Kouatchou, J., Putman, W. M., Thompson, M. A., Trayanov, A. L., Molod, A. M., Martin, R. V., and Jacob, D. J.: GEOS-Chem High Performance (GCHP v11-02c): a next-generation implementation of the GEOS-Chem chemical transport model for massively parallel applications, Geoscientific Model Development, 11, 2941–2953, https://doi.org/10.5194/gmd-11-2941-2018, 2018.

Faubert, P., Tiiva, P., Rinnan, Å., Michelsen, A., Holopainen, J. K., and Rinnan, R.: Doubled volatile organic compound emissions from subarctic tundra under simulated climate warming, New Phytologist, 187, 199–208, https://doi.org/10.1111/j.1469-8137.2010.03270.x, 2010.

Fisher, J. A., Jacob, D. J., Travis, K. R., Kim, P. S., Marais, E. A., Chan Miller, C., Yu, K., Zhu, L., Yantosca, R. M., Sulprizio, M. P., Mao, J., Wennberg, P. O., Crounse, J. D., Teng, A. P., Nguyen, T. B., St. Clair, J. M., Cohen, R. C., Romer, P., Nault, B. A., Wooldridge, P. J., Jimenez, J. L., Campuzano-Jost, P., Day, D. A., Hu, W., Shepson, P. B., Xiong, F., Blake, D. R., Goldstein, A. H., Misztal, P. K., Hanisco, T. F., Wolfe, G. M., Ryerson, T. B., Wisthaler, A., and

Formatted: Line spacing: single

Mikoviny, T.: Organic nitrate chemistry and its implications for nitrogen budgets in an isoprene- and monoterpene-rich atmosphere: constraints from aircraft (SEAC^{4}RS) and ground-based (SOAS) observations in the Southeast US, Atmospheric Chemistry and Physics, 16, 5969–5991, https://doi.org/10.5194/acp-16-5969-2016, 2016.

Foster, P. N., Prentice, I. C., Morfopoulos, C., Siddall, M., and van Weele, M.: Isoprene emissions track the seasonal cycle of canopy temperature, not primary production: evidence from remote sensing, Biogeosciences, 11, 3437–3451, https://doi.org/10.5194/bg-11-3437-2014, 2014.

Frankenberg, C., Fisher, J. B., Worden, J., Badgley, G., Saatchi, S. S., Lee, J.-E., Toon, G. C., Butz, A., Jung, M., Kuze, A., and Yokota, T.: New global observations of the terrestrial carbon cycle from GOSAT: Patterns of plant fluorescence with gross primary productivity, Geophysical Research Letters, 38, https://doi.org/10.1029/2011GL048738, 2011.

Fu, T.-M., Jacob, D. J., Palmer, P. I., Chance, K., Wang, Y. X., Barletta, B., Blake, D. R., Stanton, J. C., and Pilling, M. J.: Space-based formaldehyde measurements as constraints on volatile organic compound emissions in east and south Asia and implications for ozone, Journal of Geophysical Research: Atmospheres, 112, https://doi.org/10.1029/2006JD007853, 2007.

GEOS-Chem, T. I. G.-C.: geoschem/geos-chem: GEOS-Chem 12.7.2, , https://doi.org/10.5281/zenodo.3701669, 2020.

Giglio, L., Randerson, J. T., and Werf, G. R. van der: Analysis of daily, monthly, and annual burned area using the fourth-generation global fire emissions database (GFED4), Journal of Geophysical Research: Biogeosciences, 118, 317–328, https://doi.org/10.1002/jgrg.20042, 2013.

Gilbert, R. O.: Statistical Methods for Environmental Pollution Monitoring, John Wiley & Sons, 354 pp., 1987.

González Abad, G.: OMPS-NPP L2 NM Formaldehyde (HCHO) Total Column swath orbital V1 (OMPS_NPP_NMHCHO_L2 1), 2022.

González Abad, G., Liu, X., Chance, K., Wang, H., Kurosu, T. P., and Suleiman, R.: Updated Smithsonian Astrophysical Observatory Ozone Monitoring Instrument (SAO OMI) formaldehyde retrieval, Atmos. Meas. Tech., 8, 19–32, https://doi.org/10.5194/amt-8-19-2015, 2015.

González Abad, G., Vasilkov, A., Seftor, C., Liu, X., and Chance, K.: Smithsonian Astrophysical Observatory Ozone Mapping and Profiler Suite (SAO OMPS) formaldehyde retrieval, Atmospheric Measurement Techniques, 9, 2797–2812, https://doi.org/10.5194/amt-9-2797-2016, 2016.

González Abad, G. G., Ayazpour, Z., Kwon, H.-A., Nowlan, C. R., Miller, C. E., Chong, H., Sun, K., Vigouroux, C., Liu, X., and Chance, K.: OMI Collection 4 Formaldehyde Retrievals: Towards a Multi-Sensor, Multi-Satellite and Multi-Decadal Dataset, in: Fall Meeting 2022, 2022.

Formatted: Line spacing: single

Formatted: Line spacing: single

de Graaf, M., Sihler, H., Tilstra, L. G., and Stammes, P.: How big is an OMI pixel?, Atmospheric Measurement Techniques, 9, 3607–3618, https://doi.org/10.5194/amt-9-3607-2016, 2016.

Guenther, A., Karl, T., Harley, P., Wiedinmyer, C., Palmer, P. I., and Geron, C.: Estimates of global terrestrial isoprene emissions using MEGAN (Model of Emissions of Gases and Aerosols from Nature), Atmos. Chem. Phys., 31, 2006.

Guenther, A. B., Jiang, X., Heald, C. L., Sakulyanontvittaya, T., Duhl, T., Emmons, L. K., and Wang, X.: The Model of Emissions of Gases and Aerosols from Nature version 2.1 (MEGAN2.1): an extended and updated framework for modeling biogenic emissions, Geoscientific Model Development, 5, 1471–1492, https://doi.org/10.5194/gmd-5-1471-2012, 2012.

Hakola, H., Tarvainen, V., Laurila, T., Hiltunen, V., Hellén, H., and Keronen, P.: Seasonal variation of VOC concentrations above a boreal coniferous forest, Atmospheric Environment, 37, 1623–1634, https://doi.org/10.1016/S1352-2310(03)00014-1, 2003.

Hakola, H., Taipale, D., Praplan, A., Schallhart, S., Thomas, S., Tykkä, T., Helin, A., Bäck, J., and Hellén, H.: Emissions of volatile organic compounds from Norway spruce and potential atmospheric impacts, Frontiers in Forests and Global Change, 6, 2023.

Harrison, S. P., Morfopoulos, C., Dani, K. G. S., Prentice, I. C., Arneth, A., Atwell, B. J., Barkley, M. P., Leishman, M. R., Loreto, F., Medlyn, B. E., Niinemets, Ü., Possell, M., Peñuelas, J., and Wright, I. J.: Volatile isoprenoid emissions from plastid to planet, New Phytologist, 197, 49–57, https://doi.org/10.1111/nph.12021, 2013.

Hellén, H., Schallhart, S., Praplan, A. P., Tykkä, T., Aurela, M., Lohila, A., and Hakola, H.: Sesquiterpenes dominate monoterpenes in northern wetland emissions, Atmospheric Chemistry and Physics, 20, 7021–7034, https://doi.org/10.5194/acp-20-7021-2020, 2020.

Holmes, C. D., Prather, M. J., Søvde, O. A., and Myhre, G.: Future methane, hydroxyl, and their uncertainties: key climate and emission parameters for future predictions, Atmospheric Chemistry and Physics, 13, 285–302, https://doi.org/10.5194/acp-13-285-2013, 2013.

Hu, L., Millet, D. B., Baasandorj, M., Griffis, T. J., Turner, P., Helmig, D., Curtis, A. J., and Hueber, J.: Isoprene emissions and impacts over an ecological transition region in the U.S. Upper Midwest inferred from tall tower measurements, Journal of Geophysical Research: Atmospheres, 120, 3553–3571, https://doi.org/10.1002/2014JD022732, 2015.

Janson, R., De Serves, C., and Romero, R.: Emission of isoprene and carbonyl compounds from a boreal forest and wetland in Sweden, Agricultural and Forest Meteorology, 98–99, 671–681, https://doi.org/10.1016/S0168-1923(99)00134-3, 1999.

Jin, L., Permar, W., Selimovic, V., Ketcherside, D., Yokelson, R. J., Hornbrook, R. S., Apel, E. C., Ku, I.-T., Collett Jr., J. L., Sullivan, A. P., Jaffe, D. A., Pierce, J. R., Fried, A., Coggon, M. M., Gkatzelis, G. I., Warneke, C., Fischer, E. V., and Hu, L.: Constraining emissions of volatile organic compounds from western US wildfires with WE-CAN and FIREX-AQ airborne

Formatted: Line spacing: single

Formatted: Line spacing: single

observations, Atmospheric Chemistry and Physics, 23, 5969–5991, https://doi.org/10.5194/acp-23-5969-2023, 2023.

Jung, Y., González Abad, G., Nowlan, C. R., Chance, K., Liu, X., Torres, O., and Ahn, C.: Explicit Aerosol Correction of OMI Formaldehyde Retrievals, Earth and Space Science, 6, 2087–2105, https://doi.org/10.1029/2019EA000702, 2019.

Juráň, S., Pallozzi, E., Guidolotti, G., Fares, S., Šigut, L., Calfapietra, C., Alivernini, A., Savi, F., Večeřová, K., Křůmal, K., Večeřa, Z., and Urban, O.: Fluxes of biogenic volatile organic compounds above temperate Norway spruce forest of the Czech Republic, Agricultural and Forest Meteorology, 232, 500–513, https://doi.org/10.1016/j.agrformet.2016.10.005, 2017.

Kaiser, J., Jacob, D. J., Zhu, L., Travis, K. R., Fisher, J. A., González Abad, G., Zhang, L., Zhang, X., Fried, A., Crounse, J. D., Clair, J. M. S., and Wisthaler, A.: High-resolution inversion of OMI formaldehyde columns to quantify isoprene emission on ecosystem-relevant scales: application to the southeast US, Atmospheric Chemistry and Physics, 18, 5483–5497, https://doi.org/10.5194/acp-18-5483-2018, 2018.

Karl, T., Fall, R., Rosenstiel, T., Prazeller, P., Larsen, B., Seufert, G., and Lindinger, W.: On-line analysis of the 13CO2 labeling of leaf isoprene suggests multiple subcellular origins of isoprene precursors, Planta, 215, 894–905, https://doi.org/10.1007/s00425-002-0825-2, 2002.

Kelly, R., Chipman, M. L., Higuera, P. E., Stefanova, I., Brubaker, L. B., and Hu, F. S.: Recent burning of boreal forests exceeds fire regime limits of the past 10,000 years, PNAS, 110, 13055–13060, https://doi.org/10.1073/pnas.1305069110, 2013.

Kramshøj, M., Vedel-Petersen, I., Schollert, M., Rinnan, Å., Nymand, J., Ro-Poulsen, H., and Rinnan, R.: Large increases in Arctic biogenic volatile emissions are a direct effect of warming, Nature Geosci, 9, 349–352, https://doi.org/10.1038/ngeo2692, 2016.

Kroll, J. H. and Seinfeld, J. H.: Chemistry of secondary organic aerosol: Formation and evolution of low-volatility organics in the atmosphere, Atmospheric Environment, 42, 3593–3624, https://doi.org/10.1016/j.atmosenv.2008.01.003, 2008.

Kwon, H.-A., Abad, G. G., Nowlan, C. R., Chong, H., Souri, A. H., Vigouroux, C., Röhling, A., Kivi, R., Makarova, M., Notholt, J., Palm, M., Winkler, H., Té, Y., Sussmann, R., Rettinger, M., Mahieu, E., Strong, K., Lutsch, E., Yamanouchi, S., Nagahama, T., Hannigan, J. W., Zhou, M., Murata, I., Grutter, M., Stremme, W., De Mazière, M., Jones, N., Smale, D., and Morino, I.: Validation of OMPS Suomi NPP and OMPS NOAA-20 Formaldehyde Total Columns With NDACC FTIR Observations, Earth and Space Science, 10, e2022EA002778, https://doi.org/10.1029/2022EA002778, 2023.

Lappalainen, H. K., Sevanto, S., Bäck, J., Ruuskanen, T. M., Kolari, P., Taipale, R., Rinne, J., Kulmala, M., and Hari, P.: Day-time concentrations of biogenic volatile organic compounds in a boreal forest canopy and their relation to environmental and biological factors, Atmospheric Chemistry and Physics, 9, 5447–5459, https://doi.org/10.5194/acp-9-5447-2009, 2009.

Deleted: Jin, Q., Crippa, P., and Pryor, S. C.: Spatial characteristics and temporal evolution of the relationship between PM2.5 and aerosol optical depth over the eastern USA during 2003–2017, Atmospheric Environment, 239, 117718, https://doi.org/10.1016/j.atmosenv.2020.117718, 2020.¶
Jin, X., Fiore, A. M., Murray, L. T., Valin, L. C., Lamsal, L. N., Duncan, B., Folkert Boersma, K., De Smedt, I., Abad, G. G., Chance, K., and Tonnesen, G. S.: Evaluating a Space-Based Indicator of Surface Ozone-NOx-VOC Sensitivity Over Midlatitude Source Regions and Application to Decadal Trends, Journal of Geophysical Research: Atmospheres, 122, 10,439-10,461, https://doi.org/10.1002/2017JD026720, 2017.¶

Formatted: Line spacing: single

Lawrence, D. M., Oleson, K. W., Flanner, M. G., Thornton, P. E., Swenson, S. C., Lawrence, P. J., Zeng, X., Yang, Z.-L., Levis, S., Sakaguchi, K., Bonan, G. B., and Slater, A. G.: Parameterization improvements and functional and structural advances in Version 4 of the Community Land Model, J. Adv. Model. Earth Syst., 3, M03001, https://doi.org/10.1029/2011MS000045, 2011.

Levelt, P. F., van den Oord, G. H. J., Dobber, M. R., Malkki, A., Huib Visser, Johan de Vries, Stammes, P., Lundell, J. O. V., and Saari, H.: The ozone monitoring instrument, IEEE Trans. Geosci. Remote Sensing, 44, 1093–1101, https://doi.org/10.1109/TGRS.2006.872333, 2006.

Li, J., Mao, J., Min, K.-E., Washenfelder, R. A., Brown, S. S., Kaiser, J., Keutsch, F. N., Volkamer, R., Wolfe, G. M., Hanisco, T. F., Pollack, I. B., Ryerson, T. B., Graus, M., Gilman, J. B., Lerner, B. M., Warneke, C., de Gouw, J. A., Middlebrook, A. M., Liao, J., Welti, A., Henderson, B. H., McNeill, V. F., Hall, S. R., Ullmann, K., Donner, L. J., Paulot, F., and Horowitz, L. W.: Observational constraints on glyoxal production from isoprene oxidation and its contribution to organic aerosol over the Southeast United States, Journal of Geophysical Research: Atmospheres, 121, 9849–9861, https://doi.org/10.1002/2016JD025331, 2016.

Liao, J., Wolfe, G. M., Hannun, R. A., St. Clair, J. M., Hanisco, T. F., Gilman, J. B., Lamplugh, A., Selimovic, V., Diskin, G. S., Nowak, J. B., Halliday, H. S., DiGangi, J. P., Hall, S. R., Ullmann, K., Holmes, C. D., Fite, C. H., Agastra, A., Ryerson, T. B., Peischl, J., Bourgeois, I., Warneke, C., Coggon, M. M., Gkatzelis, G. I., Sekimoto, K., Fried, A., Richter, D., Weibring, P., Apel, E. C., Hornbrook, R. S., Brown, S. S., Womack, C. C., Robinson, M. A., Washenfelder, R. A., Veres, P. R., and Neuman, J. A.: Formaldehyde evolution in US wildfire plumes during the Fire Influence on Regional to Global Environments and Air Quality experiment (FIREX-AQ), Atmospheric Chemistry and Physics, 21, 18319–18331, https://doi.org/10.5194/acp-21-18319-2021, 2021.

Formatted: Line spacing: single

Lindwall, F., Schollert, M., Michelsen, A., Blok, D., and Rinnan, R.: Fourfold higher tundra volatile emissions due to arctic summer warming, Journal of Geophysical Research: Biogeosciences, 121, 895–902, https://doi.org/10.1002/2015JG003295, 2016a.

Lindwall, F., Svendsen, S. S., Nielsen, C. S., Michelsen, A., and Rinnan, R.: Warming increases isoprene emissions from an arctic fen, Science of The Total Environment, 553, 297–304, https://doi.org/10.1016/j.scitotenv.2016.02.111, 2016b.

Liu, X., Huey, L. G., Yokelson, R. J., Selimovic, V., Simpson, I. J., Müller, M., Jimenez, J. L., Campuzano-Jost, P., Beyersdorf, A. J., Blake, D. R., Butterfield, Z., Choi, Y., Crounse, J. D., Day, D. A., Diskin, G. S., Dubey, M. K., Fortner, E., Hanisco, T. F., Hu, W., King, L. E., Kleinman, L., Meinardi, S., Mikoviny, T., Onasch, T. B., Palm, B. B., Peischl, J., Pollack, I. B., Ryerson, T. B., Sachse, G. W., Sedlacek, A. J., Shilling, J. E., Springston, S., Clair, J. M. S., Tanner, D. J., Teng, A. P., Wennberg, P. O., Wisthaler, A., and Wolfe, G. M.: Airborne measurements of western U.S. wildfire emissions: Comparison with prescribed burning and air quality implications, Journal of Geophysical Research: Atmospheres, 122, 6108–6129, https://doi.org/10.1002/2016JD026315, 2017.

Magney, T. S., Bowling, D. R., Logan, B. A., Grossmann, K., Stutz, J., Blanken, P. D., Burns, S. P., Cheng, R., Garcia, M. A., Köhler, P., Lopez, S., Parazoo, N. C., Raczka, B., Schimel, D., and Frankenberg, C.: Mechanistic evidence for tracking the seasonality of photosynthesis with solar-induced fluorescence, PNAS, 116, 11640–11645, https://doi.org/10.1073/pnas.1900278116, 2019.

Mao, J., Jacob, D. J., Evans, M. J., Olson, J. R., Ren, X., Brune, W. H., Clair, J. M. S., Crounse, J. D., Spencer, K. M., Beaver, M. R., Wennberg, P. O., Cubison, M. J., Jimenez, J. L., Fried, A., Weibring, P., Walega, J. G., Hall, S. R., Weinheimer, A. J., Cohen, R. C., Chen, G., Crawford, J. H., McNaughton, C., Clarke, A. D., Jaeglé, L., Fisher, J. A., Yantosca, R. M., Le Sager, P., and Carouge, C.: Chemistry of hydrogen oxide radicals (HO_x) in the Arctic troposphere in spring, Atmospheric Chemistry and Physics, 10, 5823–5838, https://doi.org/10.5194/acp-10-5823-2010, 2010.

Mao, J., Paulot, F., Jacob, D. J., Cohen, R. C., Crounse, J. D., Wennberg, P. O., Keller, C. A., Hudman, R. C., Barkley, M. P., and Horowitz, L. W.: Ozone and organic nitrates over the eastern United States: Sensitivity to isoprene chemistry, Journal of Geophysical Research: Atmospheres, 118, 11,256-11,268, https://doi.org/10.1002/jgrd.50817, 2013.

Mao, J., Carlton, A., Cohen, R. C., Brune, W. H., Brown, S. S., Wolfe, G. M., Jimenez, J. L., Pye, H. O. T., Lee Ng, N., Xu, L., McNeill, V. F., Tsigaridis, K., McDonald, B. C., Warneke, C., Guenther, A., Alvarado, M. J., de Gouw, J., Mickley, L. J., Leibensperger, E. M., Mathur, R., Nolte, C. G., Portmann, R. W., Unger, N., Tosca, M., and Horowitz, L. W.: Southeast Atmosphere Studies: learning from model-observation syntheses, Atmospheric Chemistry and Physics, 18, 2615–2651, https://doi.org/10.5194/acp-18-2615-2018, 2018.

Marais, E. A., Jacob, D. J., Kurosu, T. P., Chance, K., Murphy, J. G., Reeves, C., Mills, G., Casadio, S., Millet, D. B., Barkley, M. P., Paulot, F., and Mao, J.: Isoprene emissions in Africa inferred from OMI observations of formaldehyde columns, Atmospheric Chemistry and Physics, 12, 6219–6235, https://doi.org/10.5194/acp-12-6219-2012, 2012.

van Meeningen, Y., Wang, M., Karlsson, T., Seifert, A., Schurgers, G., Rinnan, R., and Holst, T.: Isoprenoid emission variation of Norway spruce across a European latitudinal transect, Atmospheric Environment, 170, 45–57, https://doi.org/10.1016/j.atmosenv.2017.09.045, 2017.

Millet, D. B., Jacob, D. J., Boersma, K. F., Fu, T.-M., Kurosu, T. P., Chance, K., Heald, C. L., and Guenther, A.: Spatial distribution of isoprene emissions from North America derived from formaldehyde column measurements by the OMI satellite sensor, J. Geophys. Res., 113, D02307, https://doi.org/10.1029/2007JD008950, 2008.

Morfopoulos, C., Müller, J.-F., Stavrakou, T., Bauwens, M., De Smedt, I., Friedlingstein, P., Prentice, I. C., and Regnier, P.: Vegetation responses to climate extremes recorded by remotely sensed atmospheric formaldehyde, Global Change Biology, 28, 1809–1822, https://doi.org/10.1111/gcb.15880, 2022.

Mu, M., Randerson, J. T., van der Werf, G. R., Giglio, L., Kasibhatla, P., Morton, D., Collatz, G. J., DeFries, R. S., Hyer, E. J., Prins, E. M., Griffith, D. W. T., Wunsch, D., Toon, G. C., Sherlock, V., and Wennberg, P. O.: Daily and 3-hourly variability in global fire emissions and

Formatted: Line spacing: single

consequences for atmospheric model predictions of carbon monoxide, Journal of Geophysical Research: Atmospheres, 116, https://doi.org/10.1029/2011JD016245, 2011.

Nowlan, C. R., González Abad, G., Kwon, H.-A., Ayazpour, Z., Chan Miller, C., Chance, K., Chong, H., Liu, X., O'Sullivan, E., Wang, H., Zhu, L., De Smedt, I., Jaross, G., Seftor, C., and Sun, K.: Global Formaldehyde Products From the Ozone Mapping and Profiler Suite (OMPS) Nadir Mappers on Suomi NPP and NOAA-20, Earth and Space Science, 10, e2022EA002643, https://doi.org/10.1029/2022EA002643, 2023.

Oleson, K., Lawrence, M., Bonan, B., Drewniak, B., Huang, M., Koven, D., Levis, S., Li, F., Riley, J., Subin, M., Swenson, S., Thornton, E., Bozbiyik, A., Fisher, R., Heald, L., Kluzek, E., Lamarque, J.-F., Lawrence, J., Leung, R., Lipscomb, W., Muszala, P., Ricciuto, M., Sacks, J., Sun, Y., Tang, J., and Yang, Z.-L.: Technical description of version 4.5 of the Community Land Model (CLM), https://doi.org/10.5065/D6RR1W7M, 2013.

Palmer, P. I., Jacob, D. J., Chance, K., Martin, R. V., Spurr, R. J. D., Kurosu, T. P., Bey, I., Yantosca, R., Fiore, A., and Li, Q.: Air mass factor formulation for spectroscopic measurements from satellites: Application to formaldehyde retrievals from the Global Ozone Monitoring Experiment, J. Geophys. Res., 106, 14539–14550, https://doi.org/10.1029/2000JD900772, 2001.

Park, R. J., Jacob, D. J., Field, B. D., Yantosca, R. M., and Chin, M.: Natural and transboundary pollution influences on sulfate-nitrate-ammonium aerosols in the United States: Implications for policy, Journal of Geophysical Research: Atmospheres, 109, https://doi.org/10.1029/2003JD004473, 2004.

Permar, W., Wang, Q., Selimovic, V., Wielgasz, C., Yokelson, R. J., Hornbrook, R. S., Hills, A. J., Apel, E. C., Ku, I., Zhou, Y., Sive, B. C., Sullivan, A. P., Collett, J. L., Campos, T. L., Palm, B. B., Peng, Q., Thornton, J. A., Garofalo, L. A., Farmer, D. K., Kreidenweis, S. M., Levin, E. J. T., DeMott, P. J., Flocke, F., Fischer, E. V., and Hu, L.: Emissions of Trace Organic Gases From Western U.S. Wildfires Based on WE-CAN Aircraft Measurements, JGR Atmospheres, 126, https://doi.org/10.1029/2020JD033838, 2021.

Porcar-Castell, A., Tyystjärvi, E., Atherton, J., van der Tol, C., Flexas, J., Pfündel, E. E., Moreno, J., Frankenberg, C., and Berry, J. A.: Linking chlorophyll a fluorescence to photosynthesis for remote sensing applications: mechanisms and challenges, J Exp Bot, 65, 4065–4095, https://doi.org/10.1093/jxb/eru191, 2014.

Potosnak, M. J., Baker, B. M., LeStourgeon, L., Disher, S. M., Griffin, K. L., Bret-Harte, M. S., and Starr, G.: Isoprene emissions from a tundra ecosystem, Biogeosciences, 10, 871–889, https://doi.org/10.5194/bg-10-871-2013, 2013.

Randerson, J. T., VAN DER WERF, G. R., GIGLIO, L., COLLATZ, G. J., and KASIBHATLA, P. S.: Global Fire Emissions Database, Version 4.1 (GFEDv4), 1925.7122549999906 MB, https://doi.org/10.3334/ORNLDAAC/1293, 2017.

Rantala, P., Aalto, J., Taipale, R., Ruuskanen, T. M., and Rinne, J.: Annual cycle of volatile organic compound exchange between a boreal pine forest and the atmosphere, Biogeosciences, 12, 5753–5770, https://doi.org/10.5194/bg-12-5753-2015, 2015.

Formatted: Line spacing: single

Formatted: Line spacing: single

Riedel, K., Weller, R., and Schrems, O.: Variability of formaldehyde in the Antarctic troposphere, Phys. Chem. Chem. Phys., 1, 5523–5527, https://doi.org/10.1039/a905368i, 1999.

Rienecker, M. M., Suarez, M. J., Gelaro, R., Todling, R., Bacmeister, J., Liu, E., Bosilovich, M. G., Schubert, S. D., Takacs, L., Kim, G.-K., Bloom, S., Chen, J., Collins, D., Conaty, A., da Silva, A., Gu, W., Joiner, J., Koster, R. D., Lucchesi, R., Molod, A., Owens, T., Pawson, S., Pegion, P., Redder, C. R., Reichle, R., Robertson, F. R., Ruddick, A. G., Sienkiewicz, M., and Woollen, J.: MERRA: NASA's Modern-Era Retrospective Analysis for Research and Applications, J. Climate, 24, 3624–3648, https://doi.org/10.1175/JCLI-D-11-00015.1, 2011.

Rinne, J., Hakola, H., Laurila, T., and Rannik, Ü.: Canopy scale monoterpene emissions of Pinus sylvestris dominated forests, Atmospheric Environment, 34, 1099–1107, https://doi.org/10.1016/S1352-2310(99)00335-0, 2000.

Schollert, M., Burchard, S., Faubert, P., Michelsen, A., and Rinnan, R.: Biogenic volatile organic compound emissions in four vegetation types in high arctic Greenland, Polar Biol, 37, 237–249, https://doi.org/10.1007/s00300-013-1427-0, 2014.

Seco, R., Holst, T., Davie-Martin, C. L., Simin, T., Guenther, A., Pirk, N., Rinne, J., and Rinnan, R.: Strong isoprene emission response to temperature in tundra vegetation, Proceedings of the National Academy of Sciences, 119, e2118014119, https://doi.org/10.1073/pnas.2118014119, 2022.

Selimovic, V., Ketcherside, D., Chaliyakunnel, S., Wielgasz, C., Permar, W., Angot, H., Millet, D. B., Fried, A., Helmig, D., and Hu, L.: Atmospheric biogenic volatile organic compounds in the Alaskan Arctic tundra: constraints from measurements at Toolik Field Station, Atmospheric Chemistry and Physics, 22, 14037–14058, https://doi.org/10.5194/acp-22-14037-2022, 2022.

Smedt, I., Müller, J.-F., Stavrakou, T., van der A, R., Eskes, H., and Van Roozendael, M.: Twelve years of global observations of formaldehyde in the troposphere using GOME and SCIAMACHY sensors, Atmospheric Chemistry and Physics, 8, 4947–4963, https://doi.org/10.5194/acp-8-4947-2008, 2008.

Smedt, I. D., Theys, N., Yu, H., Danckaert, T., Lerot, C., Compernolle, S., Roozendael, M. V., Richter, A., Hilboll, A., Peters, E., Pedergnana, M., Loyola, D., Beirle, S., Wagner, T., Eskes, H., Geffen, J. van, Boersma, K. F., and Veefkind, P.: Algorithm theoretical baseline for formaldehyde retrievals from S5P TROPOMI and from the QA4ECV project, Atmospheric Measurement Techniques, 11, 2395–2426, https://doi.org/10.5194/amt-11-2395-2018, 2018.

Spirig, C., Guenther, A., Greenberg, J. P., Calanca, P., and Tarvainen, V.: Tethered balloon measurements of biogenic volatile organic compounds at a Boreal forest site, Atmospheric Chemistry and Physics, 4, 215–229, https://doi.org/10.5194/acp-4-215-2004, 2004.

Stavrakou, T., Müller, J.-F., De Smedt, I., Van Roozendael, M., van der Werf, G. R., Giglio, L., and Guenther, A.: Evaluating the performance of pyrogenic and biogenic emission inventories against one decade of space-based formaldehyde columns, Atmospheric Chemistry and Physics, 9, 1037–1060, https://doi.org/10.5194/acp-9-1037-2009, 2009.

Formatted: Line spacing: single

Stavrakou, T., Müller, J.-F., Bauwens, M., De Smedt, I., Van Roozendael, M., De Mazière, M., Vigouroux, C., Hendrick, F., George, M., Clerbaux, C., Coheur, P.-F., and Guenther, A.: How consistent are top-down hydrocarbon emissions based on formaldehyde observations from GOME-2 and OMI?, Atmos. Chem. Phys., 15, 11861–11884, https://doi.org/10.5194/acp-15-11861-2015, 2015.

Stavrakou, T., Müller, J.-F., Bauwens, M., Smedt, I. D., Roozendael, M. V., and Guenther, A.: Impact of Short-Term Climate Variability on Volatile Organic Compounds Emissions Assessed Using OMI Satellite Formaldehyde Observations, Geophysical Research Letters, 45, 8681–8689, https://doi.org/10.1029/2018GL078676, 2018.

Tang, J., Schurgers, G., Valolahti, H., Faubert, P., Tiiva, P., Michelsen, A., and Rinnan, R.: Challenges in modelling isoprene and monoterpene emission dynamics of Arctic plants: a case study from a subarctic tundra heath, Biogeosciences, 13, 6651–6667, https://doi.org/10.5194/bg-13-6651-2016, 2016.

Tiiva, P., Faubert, P., Michelsen, A., Holopainen, T., Holopainen, J. K., and Rinnan, R.: Climatic warming increases isoprene emission from a subarctic heath, New Phytologist, 180, 853–863, https://doi.org/10.1111/j.1469-8137.2008.02587.x, 2008.

Timkovsky, I. I., Elanskii, N. F., Skorokhod, A. I., and Shumskii, R. A.: Studying of biogenic volatile organic compounds in the atmosphere over Russia, Izv. Atmos. Ocean. Phys., 46, 319–327, https://doi.org/10.1134/S0001433810030059, 2010.

Travis, K. R., Jacob, D. J., Fisher, J. A., Kim, P. S., Marais, E. A., Zhu, L., Yu, K., Miller, C. C., Yantosca, R. M., Sulprizio, M. P., and others: Why do models overestimate surface ozone in the Southeast United States?, Atmospheric Chemistry and Physics, 16, 13561–13577, 2016.

Valolahti, H., Kivimäenpää, M., Faubert, P., Michelsen, A., and Rinnan, R.: Climate change-induced vegetation change as a driver of increased subarctic biogenic volatile organic compound emissions, Global Change Biology, 21, 3478–3488, https://doi.org/10.1111/gcb.12953, 2015.

Vedel-Petersen, I., Schollert, M., Nymand, J., and Rinnan, R.: Volatile organic compound emission profiles of four common arctic plants, Atmospheric Environment, 120, 117–126, https://doi.org/10.1016/j.atmosenv.2015.08.082, 2015.

Vigouroux, C., Langerock, B., Bauer Aquino, C. A., Blumenstock, T., Mazière, M. D., Smedt, I. D., Grutter, M., Hannigan, J., Jones, N., Kivi, R., Lutsch, E., Mahieu, E., Makarova, M., Metzger, J.-M., Morino, I., Murata, I., Nagahama, T., Notholt, J., Ortega, I., Palm, M., Pinardi, G., Röhling, A., Smale, D., Stremme, W., Strong, K., Sussmann, R., Té, Y., Roozendael, M. van, Wang, P., and Winkler, H.: TROPOMI/S5P formaldehyde validation using an extensive network of ground-based FTIR stations, Atmospheric Measurement Techniques Discussions, 1–24, https://doi.org/10.5194/amt-2020-30, 2020.

Wang, M., Schurgers, G., Arneth, A., Ekberg, A., and Holst, T.: Seasonal variation in biogenic volatile organic compound (BVOC) emissions from Norway spruce in a Swedish boreal forest, BOREAL ENVIRONMENT RESEARCH, 22, 353–367, 2017.

van der Werf, G. R., Randerson, J. T., Giglio, L., van Leeuwen, T. T., Chen, Y., Rogers, B. M., Mu, M., van Marle, M. J. E., Morton, D. C., Collatz, G. J., Yokelson, R. J., and Kasibhatla, P. S.: Global fire emissions estimates during 1997–2016, Earth Syst. Sci. Data, 9, 697–720, https://doi.org/10.5194/essd-9-697-2017, 2017.

Wolfe, G. M., Kaiser, J., Hanisco, T. F., Keutsch, F. N., de Gouw, J. A., Gilman, J. B., Graus, M., Hatch, C. D., Holloway, J., Horowitz, L. W., Lee, B. H., Lerner, B. M., Lopez-Hilifiker, F., Mao, J., Marvin, M. R., Peischl, J., Pollack, I. B., Roberts, J. M., Ryerson, T. B., Thornton, J. A., Veres, P. R., and Warneke, C.: Formaldehyde production from isoprene oxidation across NOx regimes, Atmos Chem Phys, 16, 2597–2610, https://doi.org/10.5194/acp-16-2597-2016, 2016.

Yu, L., Wen, J., Chang, C. Y., Frankenberg, C., and Sun, Y.: High Resolution Global Contiguous SIF Estimates from OCO-2 SIF and MODIS, Version 2, ORNL DAAC, https://doi.org/10.3334/ORNLDAAC/1863, 2021.

Yurganov, L. and Rakitin, V.: Two Decades of Satellite Observations of Carbon Monoxide Confirm the Increase in Northern Hemispheric Wildfires, Atmosphere, 13, 1479, https://doi.org/10.3390/atmos13091479, 2022.

Zhang, Y., Li, R., Min, Q., Bo, H., Fu, Y., Wang, Y., and Gao, Z.: The Controlling Factors of Atmospheric Formaldehyde (HCHO) in Amazon as Seen From Satellite, Earth and Space Science, 6, 959–971, https://doi.org/10.1029/2019EA000627, 2019.

Zhao, T.: Data used in the work “Zhao and Mao 2023: Interannual variability of summertime formaldehyde (HCHO) vertical column density and its main drivers in northern high latitudes,” https://doi.org/10.6084/m9.figshare.23599566.v1, 2023a.

Zhao, T.: Holton1/Codes-for-HCHO-interannual-variability-in-northern-high-latitudes: Interannual variability of summertime formaldehyde (HCHO) vertical column density and its main drivers in northern high latitudes, , https://doi.org/10.5281/zenodo.8094844, 2023b.

Zhao, T., Mao, J., Simpson, W. R., De Smedt, I., Zhu, L., Hanisco, T. F., Wolfe, G. M., St. Clair, J. M., González Abad, G., Nowlan, C. R., Barletta, B., Meinardi, S., Blake, D. R., Apel, E. C., and Hornbrook, R. S.: Source and variability of formaldehyde (HCHO) at northern high latitudes: an integrated satellite, aircraft, and model study, Atmos. Chem. Phys., 22, 7163–7178, https://doi.org/10.5194/acp-22-7163-2022, 2022.

Zheng, Y., Unger, N., Barkley, M. P., and Yue, X.: Relationships between photosynthesis and formaldehyde as a probe of isoprene emission, Atmos. Chem. Phys. Discuss., 15, 11763–11797, https://doi.org/10.5194/acpd-15-11763-2015, 2015.

Zheng, Y., Unger, N., Tadić, J. M., Seco, R., Guenther, A. B., Barkley, M. P., Potosnak, M. J., Murray, L. T., Michalak, A. M., Qiu, X., Kim, S., Karl, T., Gu, L., and Pallardy, S. G.: Drought impacts on photosynthesis, isoprene emission and atmospheric formaldehyde in a mid-latitude forest, Atmospheric Environment, 167, 190–201, https://doi.org/10.1016/j.atmosenv.2017.08.017, 2017.

Formatted: Line spacing: single

Zheng, Y., Thornton, J. A., Ng, N. L., Cao, H., Henze, D. K., McDuffie, E. E., Hu, W., Jimenez, J. L., Marais, E. A., Edgerton, E., and Mao, J.: Long-term observational constraints of organic aerosol dependence on inorganic species in the southeast US, Atmospheric Chemistry and Physics, 20, 13091–13107, https://doi.org/10.5194/acp-20-13091-2020, 2020.

Zhou, P., Ganzeveld, L., Taipale, D., Rannik, Ü., Rantala, P., Rissanen, M. P., Chen, D., and Boy, M.: Boreal forest BVOCs exchange: emissions versus in-canopy sinks, Gases/Atmospheric Modelling/Troposphere/Physics (physical properties and processes), https://doi.org/10.5194/acp-2017-493, 2017.

Zhu, L., Jacob, D. J., Kim, P. S., Fisher, J. A., Yu, K., Travis, K. R., Mickley, L. J., Yantosca, R. M., Sulprizio, M. P., Smedt, I. D., González Abad, G., Chance, K., Li, C., Ferrare, R., Fried, A., Hair, J. W., Hanisco, T. F., Richter, D., Jo Scarino, A., Walega, J., Weibring, P., and Wolfe, G. M.: Observing atmospheric formaldehyde (HCHO) from space: validation and intercomparison of six retrievals from four satellites (OMI, GOME2A, GOME2B, OMPS) with SEAC^{4}RS aircraft observations over the southeast US, Atmospheric Chemistry and Physics, 16, 13477–13490, https://doi.org/10.5194/acp-16-13477-2016, 2016.

Zhu, L., González Abad, G., Nowlan, C. R., Chan Miller, C., Chance, K., Apel, E. C., DiGangi, J. P., Fried, A., Hanisco, T. F., Hornbrook, R. S., Hu, L., Kaiser, J., Keutsch, F. N., Permar, W., St. Clair, J. M., and Wolfe, G. M.: Validation of satellite formaldehyde (HCHO) retrievals using observations from 12 aircraft campaigns, Atmos. Chem. Phys., 20, 12329–12345, https://doi.org/10.5194/acp-20-12329-2020, 2020.

Page 16: [1] Deleted	**Tianlang Zhao**	**2/5/24 4:02:00 AM**

Page 16: [2] Deleted	**Tianlang Zhao**	**2/5/24 4:02:00 AM**

Page 16: [3] Deleted	**Tianlang Zhao**	**2/5/24 4:02:00 AM**

Page 16: [4] Deleted	**Tianlang Zhao**	**2/5/24 4:02:00 AM**

Page 16: [5] Deleted	**Tianlang Zhao**	**2/5/24 4:02:00 AM**

Page 16: [6] Deleted	**Tianlang Zhao**	**2/5/24 4:02:00 AM**

Page 16: [7] Deleted	**Tianlang Zhao**	**2/5/24 4:02:00 AM**

Page 16: [8] Deleted	**Tianlang Zhao**	**2/5/24 4:02:00 AM**